Journal of Petroleum Science and Engineering 205 (2021) 108801

Contents lists available at ScienceDirect

Journal of Petroleum Science and Engineering

journal homepage: http://www.elsevier.com/locate/petrol

Experimental and modelling approach to investigate the mechanisms of formation damage due to calcium carbonate precipitation in carbonate reservoirs

Sajjad Qazvini [a], Abdolah Golkari [b], Amin Azdarpour [a,*], Rafael M. Santos [c], Mir Saeid Safavi [a], Milad Norouzpour [a]

[a] Department of Petroleum Engineering, Marvdasht Branch, Islamic Azad University, Marvdasht, Iran
[b] Department of Chemical Engineering, School of Chemical and Petroleum Engineering, Shiraz University, Shiraz, Iran
[c] School of Engineering, University of Guelph, 50 Stone Road East, Guelph, N1G 2W1, Ontario, Canada

ARTICLE INFO

Keywords:
$CaCO_3$ scale formation
OLI Software
Carbonate reservoir
Water flooding
Low flow rate
Permeability reduction
Turbidity

ABSTRACT

Calcium carbonate ($CaCO_3$) precipitation, due to incompatibility between the injected water (IW) and formation water (FW), is known to be a major operational obstacle during water flooding projects. In this study, initially by using OLI Scale Chem and ScaleSoftPitzer software and static beaker tests, the potentiality of $CaCO_3$ scaling was determined from the given ionic content of incompatible synthetic brines, under different conditions (temperature, pressure, and volume mixing ratio of incompatible brines). The results showed that the maximum amount of $CaCO_3$ salt was formed at a volume mixing ratio of 0.8:0.2 (IW:FW). The simulation results showed that OLI software is more reliable than the ScaleSoftPitzer. In the second stage of this work, the 0.8:0.2 proportion of IW:FW was selected to examine the mechanisms under which the maximum formation damage of the tight carbonate cores occurred through the water injection experiments. In addition, the turbidity of the bulk solution was measured to confirm the core flooding outcomes. Various hydrodynamic parameters (low flow rate, scaling tendency, and the temperature) were evaluated in these experiments. Bulk induction time (t_{ind}) and scaling period (t_s) were determined from the setup. Either heterogeneous nucleation (i.e. crystallization processes), or both heterogeneous nucleation and adhesion of pre-deposited crystals from the mixed incompatible brines to the pore wall of the cores, were attributed as the principal mechanisms of the formation damage of tight carbonate rocks owing to $CaCO_3$ salt formation. Moreover, a semi-empirical model was established from this laboratory study, which predicts the scaling period (t_s) as a function of interfacial energy, temperature, and scaling tendencies.

1. Introduction

Despite society's best attempts towards growing renewable energy sources, more than 70% of the global energy consumption in the last few decades is expected to come from fossil fuels (Birol et al., 2015). The demand for oil and natural gas has continued to increase with increasing global energy utilization. Water-flooding for maintaining the pressure and enhancing secondary recovery from mature fields is one of the economically feasible approaches for water-driven reservoirs. The used water must be treated and chemically adjusted before injection. However, the injected water may reduce the permeability or cause formation damage by fluid-formation or fluid-fluid interactions (Haghtalab et al., 2015; Moghadasi et al., 2004b). Formation damage in water injection systems is determined by different complex and coupled phenomena, which decrease the permeability of reservoir rocks. A particular and well-known mechanisms of formation damage emerges when an incompatible brine is injected into a reservoir. An appreciable amount of low solubility minerals may precipitate away from the mixture causing scale formation, thus plugging flow channels that may be rendered impermeable to any fluids.

During the water-flooding process, inorganic deposit scales are one of the most drastic types of formation damage. The scale deposit can lead to clogging and hinder fluid flow in the formation, wellbore, tubing, casing, topside production facilities, pipelines, valves, perforations, and

* Corresponding author.
E-mail addresses: amin.azhdarpour@miau.ac.ir, aminazh22@gmail.com (A. Azdarpour).

https://doi.org/10.1016/j.petrol.2021.108801
Received 26 June 2020; Received in revised form 22 February 2021; Accepted 9 April 2021
Available online 13 April 2021

downhole devices. These phenomena can result in a significant increase in pressure drop, and ultimately it reduces the productivity of the wells, which leads to a considerable treatment cost and deterioration of the oil extraction process. Precipitation of inorganic salts in the reservoir rock pores during the water injection process is the main reason for the decrease in the injectivity over time (BinMerdhah et al., 2010). The conventional oilfield scales are classified as sulfates, carbonates, sulfides (generally iron sulfides), and oxides (mainly iron oxides), and their likelihood for formation differs from one oilfield to another. The presence of ions in the water plays a significant role in the type of scale formed in the oilfields (Kamal et al., 2018).

Inorganic scales can be categorized based on their sensitivity to pH. Sulfate scales ($CaSO_4$, $BaSO_4$, and $SrSO_4$) are not sensitive to pH, as they cannot be readily dissolved by acids, while the scaling tendency of carbonates is strongly influenced by the pH of brines, as they are acid-soluble. The precipitation rate of carbonate scales is difficult to predict since $CaCO_3$ is a pH-dependent scale (Kan and Tomson, 2012). As such, one of the most widely studied inorganic scales frequently encountered in oil field operations is calcium carbonate or calcite. A fundamental study of the chemical reactions between brine and CO_2 (in the gas phase) is necessary for $CaCO_3$ scaling prediction in water-flooding operations. Carbon dioxide and carbonate mineral generally exist in most carbonate reservoirs; therefore, under reservoir conditions, the FW is typically saturated with $CaCO_3$. Based on the following ionization equations, carbonic acid forms once CO_2 dissolves in water:

$$CO_2 + H_2O \leftrightarrow H_2CO_3$$

$$H_2CO_3 \leftrightarrow H^+ + HCO_3^-,$$

$$HCO_3^- \leftrightarrow CO_3^{-2} + H^+$$

The hydrogen ion and bicarbonate ion created from the carbonic acid ionizes. As the first ionization constant of carbonic acid is much larger than the second ionization constant, bicarbonate ions are more numerous than carbonate ions under typical FW situation. Hence, the deposition of $CaCO_3$ can be generally indicated as follows:

$$Ca^{+2} + 2HCO_3^- \leftrightarrow Ca(HCO_3)_2 \leftrightarrow H_2O + CO_2 + CaCO_3$$

From the Le Chatelier assumption, more calcium bicarbonate is formed by an increment of the concentration of carbon dioxide. A decrease in the formation of $CaCO_3$ would result in a CO_2 increase in this system at equilibrium (Moghadasi et al., 2004a). The content of CO_2 that is in dynamic equilibrium with a given amount of HCO_3^- and CO_3^{2-} ions has a significant role in calcium carbonate solubility. As pressure is lowered, the CO_2 released from produced water can lead to an increase in water pH and consequently greater scaling tendency of the brine solution (Aziz et al., 2011; Zahedzadeh et al., 2014). Gas released from the brine solution owing to pressure drop results in the appearance of multiple two-phase flow interfaces during phase separation, which creates a suitable condition for the nucleation and crystal growth of $CaCO_3$ (Abdel-Aal et al., 2002; Chibowski et al., 2003). The amount of CO_2 content in highly mineralized solutions is challenging to experimentally determine. However, with knowledge of hydrogen ion concentrations from pH measurement, the quantitative correlation between CO_2, HCO_3^-, and CO_3^{2-} (carbonic acid/carbonate equilibrium) can be calculated. When brines have been saturated with calcium carbonate, the salt precipitation potentiality can be predicted by comparing the calculated value of pH and the real pH of the brine. (Aziz et al., 2011).

$CaCO_3$ crystallization is manifested in different stages. The first stage is ion-pairing, in which cationic (Ca^{2+}) and anionic (CO_3^{2-}) ions come into collision in solution, which creates micro-aggregates. In the second stage, nucleation sites for crystallization are formed from the growth of these micro-aggregates. Adherent macro-crystals create by a combination of these larger agglomerate microcrystals. Finally, scale film creation on the pore-wall of the reservoir rocks occurs via adsorption and grows with more scaling ions from the incompatible fluids. $CaCO_3$ formation is highly dependent on the temperature and scaling tendency of mixed injection brines (Duggirala, 2005). The induction period of salt crystallization is the time between the appearances of supersaturation and the formation of stable nuclei of the salt-forming ions. During this time, many changes in the concentration of the incompatible brines would occur, which could prevent precipitation of inorganic salts to happen. The induction period is significantly affected by the existence of impurities, the degree of agitation, viscosity, and level of the supersaturation of the mixed injected brine (Mullin, 2001; Østvold and Randhol, 2001; Verdoes et al., 1992). The crystallization mechanism is dependent on the induction period from the moment of blending the injection and formation water until the inorganic scales are detectable. The induction period decreases by increasing the scaling tendency of mixed brine. At a certain degree of scaling tendency of mixed brine, spontaneous crystallization occurs, in which a metastable solution turns into an unstable solution (Chen et al., 2005b).

The induction period of $CaCO_3$ salt formation is also dependent on the fluid injection rate, which is one of the most influential factors affecting the crystal growth rate. At a constant level of scaling tendency of mixed brine and temperature, the crystallization rate can differ greatly by changes in flow rate (Aziz et al., 2011; Mackay et al., 2005). Static beaker tests are usually the first choice to predict scale deposition under static conditions. Estimation of salt deposition under field conditions is performed with these tests due to simple equipment requirement and absence of the need for pressure control (Sousa et al., 2016). Dynamic block tubing tests are widely used to investigate the scaling phenomena and examine scale inhibitors under dynamic conditions. Differential pressure is generally measured through the working section of these tests to study the formation of scales. Scaling time is determined by measuring the time for increasing pressure drop across the working section (Al-Roomi et al., 2015; Bazin et al., 2005; X. Liu et al., 2012). The main drawback of this methodology is that it does not involve porous media to evaluate the mechanisms in which $CaCO_3$ salt is formed within reservoir rocks.

Given an identical initial permeability of rock samples, permeability reduction owing to the formation of inorganic salts can vary based on the temperature and flow rate during flooding tests (Haghtalab et al., 2015; Moghadasi et al., 2004b). The kinetics of the reaction of the calcium carbonate salt is a function of temperature (e.g. slow kinetics at low temperature). Nuclei are generated more readily at a higher temperature; they grow more quickly into particles, and the metastable area becomes narrower. Experimental works have confirmed that as the temperature increases, the formation of $CaCO_3$ inorganic scale may happen at an earlier stage (Dawe and Zhang, 1997; He et al., 1999; Ramstad et al., 2005). The influences of flow rate, temperature, brine concentration, and pore volume injected on the permeability reduction during the water injection process have been investigated. According to experimental data, a relationship is established for predicting the permeability reduction owing to inorganic scale depositions (Tahmasebi et al., 2010). One of the most important driving forces for scale deposition is supersaturation. When the content of dissolved cations (Ca^{2+}) and anions (CO_3^{2-}) increases beyond their thermodynamic solubility limit in the mixed injection brines, this creates a high supersaturation of the solution. In this case, the system conditions alter to a thermodynamically unstable state, and $CaCO_3$ deposition will eventually appear. It is noteworthy that scale deposits may occur even when the average solution content remains under the same at the local condition (Duggirala, 2005; Nergaard and Grimholt, 2010; Steiger, 2005). The supersaturation ratio, or scaling tendency, of mixed injection brine could be used to predict the potentiality of $CaCO_3$ inorganic deposition. Scaling tendency (ST) is highly depended on temperature, pressure, and ion concentration of the solution, which is calculated generally by the following equation:

$$ST = [Ca^{2+}]\cdot[CO_3^{2-}]/K_{sp,CaCO3}$$

where ST is the scaling tendency, $[Ca^{2+}]$ indicates the concentration of calcium ion in mol/L, $[CO_3^-]$ indicates carbonate ion in mol/L, and K_{sp} is the solubility product constant of $CaCO_3$ in mol^2/L^2.

The solubility product constant is an equilibrium product of a solid dissolving in an aqueous solution, and is a function of ionic strength, ion concentration, temperature, and pressure. Therefore, the higher values of K_{sp} indicate the higher solubility of the solid particles in the solution (Kamal et al., 2018). If the scaling tendency degree is greater than one, the scale deposits are formed. Furthermore, the scaling index (SI) is calculated as follow:

$$\text{Scaling Index (SI)} = \text{Log (ST)}$$

When $SI < 0$, the solution is under-saturated, and the solid can dissolve (i.e. the salt cannot precipitate). If $SI > 0$, then the solution is super-saturated, and the salt is precipitated. In the case of $SI = 0$, the solution is in equilibrium condition with the precipitated salt (Chen et al., 2007; Moghadasi et al., 2003). Scaling tendency is dependent on the solution chemistry, and thus is the major driving force for $CaCO_3$ formation. $CaCO_3$ can be in a metastable state in solution at a high scaling tendency, while $CaCO_3$ will not precipitate in an unstable state at the lowest scaling tendency. The kinetic mechanism of $CaCO_3$ formation should be considered to predict $CaCO_3$ formation that may be a risk in oilfields (Kamari et al., 2014; Mitrouli et al., 2016).

For oilfields, scale prediction software such as OLI Scale Chem and ScaleSoftPitzer™ (SSP) have been developed to forecast the amount of scale precipitation, ST, and SI of common inorganic deposits. These programs can calculate the influence of several parameters, such as temperature, pressure, the mixing ratio of brines, total dissolved solid particles, and ion-pairing, on scale precipitation (Amiri et al., 2013; Kan and Tomson, 2012). The prediction models for estimating the potentiality of scale formation in porous media have been investigated in previous works. These models were therein able to evaluate, qualitatively, the inorganic salt deposition and the scaling tendency (Amiri et al., 2013; Shokrollahi et al., 2015; Tahmasebi et al., 2010).

According to well-studied mechanisms for the salt formation from aqueous solution through water injection, the prediction of $CaCO_3$ inorganic salt can be achieved (Ramstad et al., 2005). These mechanisms include change of calcium carbonate solubility in brine due to pressure drop, decomposition of $CaCO_3$ owing to change in chemical and physical conditions of the reservoir, and mixing incompatible injected brine with hydrocarbon (Mackay and Jordan, 2005). Understanding these mechanisms is essential for the protection of reservoir and oilfield facilities from inorganic scales. The efficiency of inhibitor injection into oil reservoirs as scale prevention additives is related to the types of mechanisms under which scale is formed in saturated mixed injected brine (Khormali et al., 2015; Kiaei and Haghtalab, 2014; Y. Liu et al., 2016; Yan et al., 2015). Kelland (2014) and Li et al. (2017) studied several scale inhibitors as control strategies of scale formation in oil and gas wells. As a rule of thumb, even after using scale inhibitors as a first control technique, scale dissolvers are needed for reducing the scales (Bin Merdhah, 2010; Lu et al., 2010; Tung et al., 2004). Inhibitors are not useful in scale prevention when the formation of scales is not forecasted correctly, or inhibitor location is non-optimal (Jordan et al., 2014).

As $CaCO_3$ scales have a very high solubility in hydrochloric acid (HCl), it is the most commonly used agent in $CaCO_3$ descaling jobs in oil wells (Al Tolaihy et al., 2010). However, for controlling the reaction rate of HCl at high-temperature conditions, some additional additives are required (Olajire, 2015). Additives such as NaOH, Na_2CO_3, and KOH can convert different acid-insoluble scales to acid-soluble compounds (Olajire, 2015). For field applications, formic acid and acetic acid are diluted to 15%; at concentrations above 15%, calcium formate and calcium acetate can precipitate as reaction products due to the limited solubility of acids (Van Domelen and Jennings Jr, 1995). Also, for dissolving calcite scale, acetic acid (10 wt%) alone is four times less efficient compared to a combination of formic acid (7 wt%) and acetic acid (5 wt %) (Hall and Dill, 1988). However, acids that can react with the carbonate rocks can also cause severe damage to the carbonate formation by decreasing the pH (Wang et al., 2013a,b). A chelating agent is an attractive alternative to organic and inorganic acids for the removal of scale from formations. The common chelating agents for $CaCO_3$ dissolving are hydroxyethyl ethylene diamine tetraacetic acid (HEDTA), and ethylene diamine tetra acetic acid (EDTA) (LePage et al., 2009). The main advantages of the chelating agents are their low corrosion rate compared to HCl, satisfactory scale dissolving power, more environmentally friendly and readily biodegradable, low sludging tendencies, and less damaging to well tubular and other downhole equipment. Yet the cost of the inorganic acids is typically lower compared to chelating agents (Almubarak et al., 2017; Bageri et al., 2017; Kamal et al., 2018).

The nature of reservoir rocks has a significant role in the water flooding process. Carbonate rock reservoirs fundamentally consist of limestone and chalks; owing to their high porosity but low permeability, and having fractures, injected water is taken through an affiliation of fracture and matrix flow. The strong propensity of carbonate rock reservoirs to have fractures leads to a higher amount of injection fluid entering the matrix than would be expected. In carbonate rocks, pores blocking can rapidly occur because of suspended solids. Consequently, injection fluid then preferentially flows into micro-fractures rather than the matrix (Mackay et al., 2003). The Kometan formation in northern Iraq, which is near to the Mishrif formation in southern Iran, has low permeability and low porosity rocks that are referred to as tight carbonate rocks in the literature (Aqrawi et al., 2010; Rashid et al., 2015).

It is known that the existence of hydrocarbons in the carbonate rock reservoirs decreases the $CaCO_3$ formation because of the adsorption of hydrocarbon components onto the pore wall of the carbonate rocks, which is accompanied by an increase in particle flocculation. Particle polarization comes from the adsorption of polar components on rock surfaces. Therefore, the existence of hydrocarbons enhances the dispersion of particles. This phenomenon is associated with the adsorption of hydrocarbons on the $CaCO_3$ particles formed, and decreases the kinetics of $CaCO_3$ precipitation (Khormali et al., 2016). Furthermore, during pressure maintenance operations, water may be injected into the aquifer zone, which consists of formation water without any hydrocarbon. In this study, due to this procedure, hydrocarbons were not present in the core samples, in order to investigate the worst formation damage of the carbonate reservoir rocks owing to $CaCO_3$ deposition.

Despite the many efforts to investigate and forecast of $CaCO_3$ inorganic scale formation, the effects of minimum low flow rate, scaling tendency of mixed injection brine, pressure, temperature, and volume mixing ratio of two incompatible brines on the mechanisms of $CaCO_3$ precipitation in tight carbonate rock reservoirs are poorly understood. In this study, the mentioned parameters were investigated during static beaker tests, using OLI and SSP software, turbidity analysis, and dynamic core flooding experiments. Understanding the mechanisms of formation damage such as crystallization, adhesion, and heterogeneous nucleation due to $CaCO_3$ scale deposition in the tight carbonate rocks at a minimum low injection rate was the major aim of this work. These analyses provide valuable information about prediction and parameters that affect the $CaCO_3$ scale formation under static and dynamic conditions. In addition, little attention has been made to establishing a model that can predict the mechanisms of $CaCO_3$ scaling in the tight carbonate rocks over a period of time. This work aimed to use a technique that simulates the field scenario to implement a predictive model in both core flooding and bulk analysis tests. A comprehensive study of the mechanisms of $CaCO_3$ scale formation can lead to the development of reliable strategies for mitigating its formation in the field and improve oil recovery with reduced deposition of salts.

2. Materials and methods

2.1. Prediction of $CaCO_3$ scale precipitation and static beaker tests

The prediction of $CaCO_3$ scaling was performed using OLI Scale Chem software, which provides a set of methods for qualitatively and quantitatively predicting deposit formation under reservoir conditions. Scaling tendency, scaling index, and the mass of the precipitation of $CaCO_3$ (mg/L) were determined from a given ionic content of injection and formation waters, when the temperature, volume mixing ratio of two incompatible brines, and pressure were altered. The ionic compositions of prepared brines in the laboratory were similar to the Persian Gulf water in the case of injection water (IW), and the water of the Mishrif formation in the Sirri Island area of the Persian Gulf in the case of formation water (FW). The salts of sodium chloride, calcium chloride, and sodium bicarbonate, supplied from Merck Germany with purity higher than 99.8%, were used for preparing synthetic IW and FW. The properties of the IW and FW have been given in Table 1. It is noteworthy that the FW contains the calcium ion, whereas the IW contains the bicarbonate ion. Mixtures of these waters are thus expected to lead to $CaCO_3$ deposition and scale formation in the oilfields.

To confirm the software analysis, the two incompatible waters were mixed in clear glass bottles and total amount of the $CaCO_3$ precipitation (mg/L) was determined by filtering and weighting at various volume mixing ratios of IW:FW (0.0:1.0, 0.1:0.9, 0.2:0.8, 0.3:0.7, 0.4:0.6, 0.5:0.5, 0.6:0.4, 0.7:0.3, 0.8:0.2, 0.9:0.1, 1.0:0.0), under different temperature conditions (25, 40, 55, 70, 90 °C), and atmospheric pressure.

In static beaker tests, synthetic IW and FW brine solutions were prepared for each experiment by dissolving the appropriate salts in distilled water. Before performing each experiment, the aqueous solution was filtered and vacuum degassed to remove any particulate materials. The experimental procedures used to determine the amount of the $CaCO_3$ deposition using beaker tests under static conditions are as follows:

1. For each run, 100 ml of FW was poured in a clean glass bottle. IW was added into the solution at the desired IW:FW volume ratio to obtain the working solution. The synthetic brines were stirred using a magnetic stirrer. The glass bottles were then capped and placed inside an oven and heated to reach the required temperature for 1 h.
2. The glass bottles were removed from the oven and immediately filtered through a filter paper of 0.2 μm pore size rating. The aggregated solid crystals on the filter paper were dried in a dehumidifying oven, and the weight of dried crystal samples was measured using an electric analytical weight balance (BinMerdhah et al., 2010; Merdhah, 2010).

For validating the accuracy of the OLI Scale Chem software, a modeling comparison to the ScaleSoftPitzer program (ScaleSoftPitzer, 2009) was performed to predict the weight of $CaCO_3$ at different temperatures and volume mixing ratios.

2.2. Apparatus and procedures for dynamic tests

The apparatus of the dynamic experiments were used to investigate the permeability reduction resulting from $CaCO_3$ formation in porous media. Turbidity measurement as a bulk analysis technique was used to acquire knowledge about the efficiency of temperature, low flow rate, and scaling tendency on $CaCO_3$ scale kinetics. A schematic diagram of the constructed apparatus is shown in Fig. 1. The setup also permitted determining the optimum performance of the scaling period and conducting accurate measurement of differential pressure. The designed apparatus was able to investigate the effect of different parameters on the permeability reduction of Iranian carbonate core plugs due to $CaCO_3$ scale formation. All of the out-crop cores were provided from the Mishrif formation in southern Iran, which had low permeability and low porosity rocks. Determining the mechanisms of the formation damage of tight carbonate rocks due to $CaCO_3$ salt precipitation under different low flow rates of incompatible brines with various scaling tendency and different temperatures were the purpose of designed dynamic tests. The apparatus descriptions is divided into two parts for the experimental test conducted: (i) core flood rig description for core plug deposition tests; (ii) rig description of bulk precipitation tests (turbidity measurement).

The formation of the scale was monitored by differential pressure measurement with a high-resolution pressure transducer, which enables the detection of a low-pressure drop variation by measuring the differential pressure across the working-section. The working-section includes a Hassler-type, stainless steel core holder. This is a rubber-sleeved core holder could withstand pressures up to 10,000 psi, subjected to an external confining pressure, into which a consolidated core plug is placed. The characteristics of the core samples are shown in Table 2 and Table 3.

As shown in Tables 2 and 3, all the core plugs had identical cross-sectional areas, and they had similar initial permeability. To inject the brines during flooding, two constant flow pumps were used in this setup. Electrolab peristaltic pumps A and B were specially designed for applications requiring a smooth flow of media at low flow rates, to inject deionized water into the two stainless steel transfer cells, to displace the IW and FW into the core samples. These pumps were operated at injection rates of 0.25–1 ml/min. Transfer cells pass the fluid to the working section and separate the deionized water from the injection brine. Each cell has a capacity of 10000 ml, with a free-floating piston that was used to store the mixing volume ratio of 0.8:0.2 of synthetic IW and FW. During all core flooding runs, the working section was placed inside a temperature-controlled water bath; it raises the solution temperature to the desired test temperature before arriving at the mixing section.

The pressure was maintained by a pressure gauge regulator leading to the effluent. When the core sample flow is blocked by precipitates, the automatic pumps shut-down, and the differential pressure as a function of time is logged by the computer, which contains a LabVIEW data acquisition system. Data analysis system equipped with channel data

Table 1
The properties of synthetic IW and FW.

Ionic concentration (mmol/L)						
Aqueous phase	pH	Na^+	Cl^-	Ca^{2+}	HCO_3^-	Total dissolved solids(mg/L)
IW	8.12	53.50	40.31	–	13.20	3464
FW	7.10	0.23	124.99	62.37	–	6936

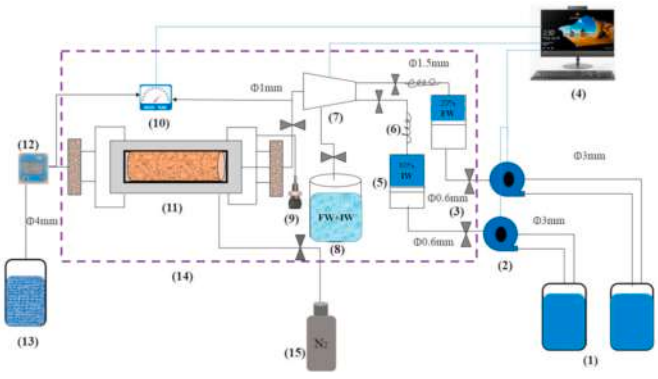

Fig. 1. Schematic diagram of the apparatus used in this study. 1) Deionized solution tanks; 2) Electrolab peristaltic pumps; 3) Valve; 4) Data acquisition system; 5) Transfer cell; 6) Spiral sections of pipe (for temperature control); 7) Mixing section; 8) Effluent sample for turbidity measurement; 9) Temperature sensor; 10) Pressure transducer; 11) Core holder; 12) Flow meter; 13) Effluent collection; 14) Thermostatic controlled bath; 15) Nitrogen cylinder.

Table 2
Porosity and permeability values for each individual core sample.

Core number	Porosity, Φ (%)	Permeability (mD)
1	15.42	10.31
2	14.60	9.90
3	15.23	11.00
4	14.76	11.25
5	13.92	10.84
6	16.64	11.30
7	16.58	9.40
8	16.53	9.20

loggers for intelligent sensors with built-in microprocessors provided automatic data recording in the form of a Microsoft Excel file. The examination of the blockage and permeability reduction of the core samples was performed based on continuous pressure increase during the core flooding experiment. These results from the differential pressure (ΔP) as a function of time across the working section gives an understanding of the $CaCO_3$ deposition kinetics.

The turbidity measurements of the mixed injection brine were carried out by creating a two-way control valve at the capillary pipe before the working section. As such, the amount of mixed brine collected could be controlled using this valve.

2.2.1. Preparation of brines for dynamic tests

The combined solution (i.e. mixing IW:FW) has a scaling tendency value greater than 1, which is analyzed in Tables 4 and 5 based on geochemical modeling, as it passes through the core samples. For the dynamic tests, the amount of reagent for preparing the brines was based on the scaling tendencies to be achieved (8, 57 and 105). The scaling tendency of brines of different compositions (varying Ca^{2+} for FW, and varying HCO_3^- for IW), at different temperatures, was calculated using OLI Scale Chem software, with precipitation disabled to be able to determine the pre-scaling ST values. The scaling tendencies desired where achieved by varying the initial composition of the brine, and were selected to cover the region between a low scaling regime to a high scaling regime, as shown in Tables 4 and 5 Brines for the dynamic test runs were then prepared for each run by dissolving the determined amounts of analytical grade of chemical salts in micro-filtered distilled water, so as to have the desired ST (before precipitation).

2.2.2. Procedure of core flooding tests

In this work, there is no oil in the system, thus all provided out-crop cores were cleaned using methanol in a soxhlet extractor and dried in an oven at 100 °C overnight before use. When the working section was filled with a tight carbonate core plug, to remove all air from the pores, a vacuum was drawn for several hours. The core was saturated with FW at ambient temperature. After the appearance of FW at the outlet, the open porosity of each carbonate core was determined, as the ratio of the required volume of FW divided by the total volume of the core. After the appearance of FW at the effluent collection, the flooding was continued through the working section until the system reached a steady state at the desired temperature and injection rate.

Experiments were performed at 60 °C and 90 °C and different low flow rates (0.25, 0.5, and 1 ml/min), and using different brine compositions. The system contains the core holder assembly with the saturated core sample. Moreover, transfer cells containing the two incompatible brines (to be mixed at a ratio of 0.8:0.2 (IW:FW)), are placed inside the thermostatic water bath and heated to the desired temperature. The system is then left for 3 h for temperature equilibrium to be attained. During each test, the solutions were injected through the core sample directly using the respective pumps. Afterward, the data acquisition system was switched on to record the experimental data. The required injection rate was adjusted by setting both supply pumps at the same low flow rates, and subsequently, the flooding run was started by turning them on to inject these $CaCO_3$ scale-forming solutions through the working section. For investigating the mechanisms of the most severe formation damage at different conditions (i.e. temperature, flow rate, and aqueous solution concentration), incompatible brine was always injected into the tight carbonate cores at a mixing ratio of 0.8:0.2 (IW:FW), since according to static beaker tests, this mixing ratio resulted in the highest amount of $CaCO_3$ precipitation. The inlet pressure was controlled by a gas cylinder and measured using the pressure transducer, while the outlet pressure was atmospheric. For investigating the formation damage due to $CaCO_3$ deposition, the ratio of permeability before and after salt precipitation was determined. In this regard, Darcy's linear flow equation was used to obtain the absolute permeability, as follows:

$$Q = (K \cdot A / \mu) \cdot (\Delta P / L) \quad (1)$$

where K is the absolute permeability of the core sample in D; Q is the injection rate of the solution in ml/min; μ is the solution viscosity in cP; L is the length of the core sample in cm; A is the cross-sectional area of the core sample in cm^2, and ΔP is the pressure drop in atm.

The core plugs were removed at the end of each flooding test, and the next run was performed with the newly prepared core sample. The apparatus was also cleaned from one run to the other by injection of an scaling-inhibitor solution of 50 wt% sodium hydroxide NaOH, and 50 wt % ethylene-diamine-acetic acid (EDTA), at a pH of 10, through the working section for about 30 min. Afterward, distilled water is injected for 2 h to remove the deposited scales. Visual static beaker test demonstrated that at this concentration of antiscalant, the desired deposited scale completely dissolved in solution. This solution was selected to prevent damage to the rock core minerals.

Table 4
OLI modeling (i.e. equilibrium concentrations without precipitation) of brine composition required to achieve the three pre-selected ST values, at 60 °C.

Brine (mmol/L)	Na^+	Cl^-	Ca^{2+}	HCO_3^-
Formation water, FW	–	125.0	5.60, 62.5, 105.0	–
Injection water, IW	53.5	–	–	8.20, 13.20, 20.50
Scaling tendency, ST (mixed 0.8:0.2 IW:FW)			8, 57, 105	8, 57, 105

Table 5
OLI modeling (i.e. equilibrium concentrations without precipitation) of brine composition required to achieve the three pre-selected ST values, at 90 °C.

Brine (mmol/L)	Na^+	Cl^-	Ca^{2+}	HCO_3^-
Formation water, FW	–	125.0	2.98, 30.63, 62.50	–
Injection water, IW	53.5	–	–	6.64, 9.84, 13.20
Scaling tendency, ST (mixed 0.8:0.2 IW:FW)			8, 57, 105	8, 57, 105

Table 3
Mean properties of the core samples.

Lithology (%)			Length, L (cm)	Diameter, D (cm)	Porosity, Φ (%)	Permeability (mD)
Calcite 80.5	Quartz 6.4	Clay 13.1	7.6	3.4	15.46	10.40

2.2.3. Turbidity measurement (bulk analysis investigation)

For studying the physical characteristics of the $CaCO_3$ scale, the bulk analysis investigation was carried out using turbidity measurements. It was conducted to confirm the formation of $CaCO_3$ in core flooding tests. Turbidity is a physical indicator of brine dispersion. It is a manifestation of the optical property that results in light being scattered and absorbed by particles or molecules instead of being transmitted in straight lines through a water sample (Lawler, 2016). The bulk induction times (t_{ind}) for $CaCO_3$ inorganic deposit to form after mixing two incompatible brines in the mixing section was determined through turbidity measurements. Every 15 min, a turbidity measurement was done for the first 90 min. Subsequently, the time interval increased to 100 min. The turbidity measurement used for this experiment is a direct method that calculates attenuation (i.e. decrease in strength) of light as it passes through a sample column of water. This method is calibrated using formazin turbidity standards, and the readings are in terms of Formazin Attenuation Units (FAU). A HI88713 Hanna turbidity meter was used in this study.

3. Results and discussion

3.1. Effect of temperature and pressure on $CaCO_3$ scale formation at different mixing ratios of IW and FW

The mass of scale formation, the scaling tendency, and the scaling index for prediction of $CaCO_3$ scale formation were investigated using OLI Scale Chem software. The results of the geochemical modeling, at atmospheric pressure, showed that $CaCO_3$ precipitation is significantly dependent on the mixing ratio of the two incompatible brines and on the temperature (Figs. 2 and 3).

The static beaker tests and ScaleSoftPitzer (Pitzer) prediction runs were performed at atmospheric pressure to determine the effect of increasing temperature at different volume mixing ratios of IW and FW on $CaCO_3$ inorganic scale formation. For the beaker tests, the solutions were filtered, and the retained scale on the filter paper was weighed in each test to support the software runs. Fig. 2 illustrates the amount of the $CaCO_3$ scale deposition, normalized per unit volume of solution (mg/L), at a volume mixing ratio of (0.4:0.6 IW:FW) and different temperatures, experimentally determined and determined by modeling. The predicted results using the OLI software and the measured actual mass of the deposition using the beaker tests were matched within an acceptable difference. At the mixing ratio of 0.4:0.6, the predicted mass of $CaCO_3$ at atmospheric pressure and temperatures of 25, 40, 55, 70, and 90 °C were approximately 130, 146, 162, 178, and 196 mg/L of solution,

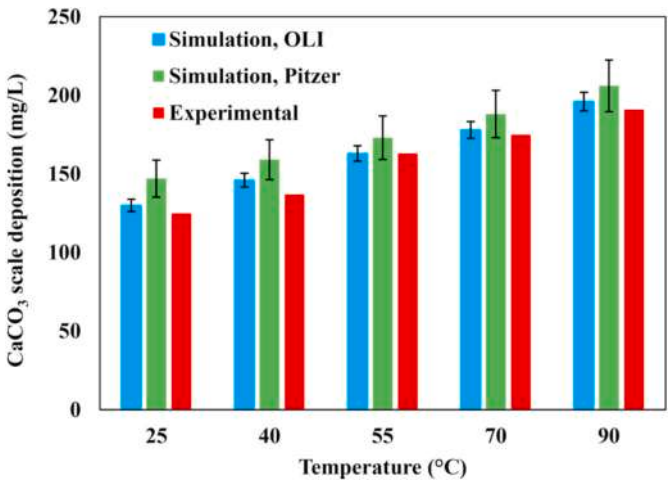

Fig. 2. Comparison of scale prediction based on modeling and static beaker tests. $CaCO_3$ scale deposition under different temperatures at the mixing ratio of 0.4:0.6 (IW:FW) and P = 1 atm.

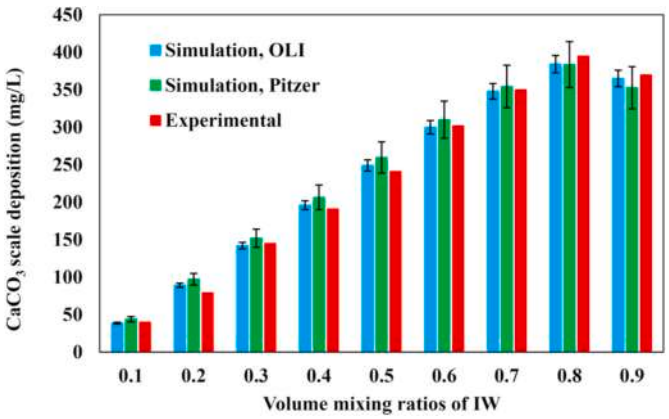

Fig. 3. Comparison of scale prediction based on modeling and static beaker tests. $CaCO_3$ scale deposition results under different volume mixing ratios at a temperature of 90 °C, and P = 1 atm.

respectively. In comparison, the experimental mass of the deposited scale under the same conditions were approximately 125, 137, 163, 175, and 191 mg/L, respectively. For this reason, the OLI Scale Chem software delivered a high precision and reliability for the prediction of scale precipitation under static conditions. Based on Fig. 2, the mean error of the beaker test and OLI prediction on the amount of $CaCO_3$ salt was less than 3%, while the mean error of the results between the static tests and the ScaleSoftPitzer program was about 8%.

Based on the modeling predictions and static beaker test results at a temperature of 90 °C (Fig. 3), the maximum amount of salt was precipitated in the solution with a volume mixing ratio of (0.8:0.2 IW:FW). These conditions represent the worst $CaCO_3$ scale scenario, as the scale amounts at 90 °C are much greater than those at 60 °C, and could lead to high permeability loss and severe formation damage in the rock samples.

Fig. 4a, b, and 4c show modeling results of the amount of $CaCO_3$ formation, scaling tendency, and scaling index of $CaCO_3$ for various mixing ratios of IW and FW and various temperatures. Based on the previous results, these analyses were performed with OLI software at a constant pressure (1 atm). As shown in Fig. 4a and b, at 90 °C, with a mixing ratio of 0.8:0.2 IW:FW, the scaling tendency of $CaCO_3$ was about 105 (i.e. much greater than 1), and the scaling index of $CaCO_3$ was about 2.0217 (i.e. much greater than 0), with about 385 mg/L of $CaCO_3$ precipitation predicted. Fig. 4c illustrates that the amount of $CaCO_3$ formation increases with increasing temperature at any mixing ratio. Therefore, it can be concluded that the precipitation of the salt is heavily temperature dependent, but is also significantly dependent on the proportion of IW and FW under reservoir conditions, owing to $CaCO_3$ being formed when FW is mixed with IW, containing high concentrations of Ca^{2+} and HCO_3^-, respectively.

Both in the software predictions and the beaker tests at a constant atmospheric pressure, the $CaCO_3$ precipitation was increased by increasing the temperature. At 25 °C and atmospheric pressure, there was little scale deposition compared with 70 °C or 90 °C. Obvious increments of deposits occurred when the test was carried out with mixing ratio of 0.8:0.2 (IW:FW) at a temperature of 90 °C. There are inconsistencies in literature, such as the study of Khormali et al. (2016), on the volume mixing ratio of IW:FW that leads to the highest amount of $CaCO_3$ deposition. Their study showed that the FW is primarily responsible for the deposition of $CaCO_3$ in carbonate reservoir and oilfield equipment, compared to injection water; that is, a high tendency of $CaCO_3$ scale formation occurred with lower amounts of injection water in mixtures with formation water in the study. In the present work, it is shown that substantial amounts of IW, compared to the FW, are needed to cause the highest amount of $CaCO_3$ deposition. This is explained by the injection water in the present study being much richer in dissolved

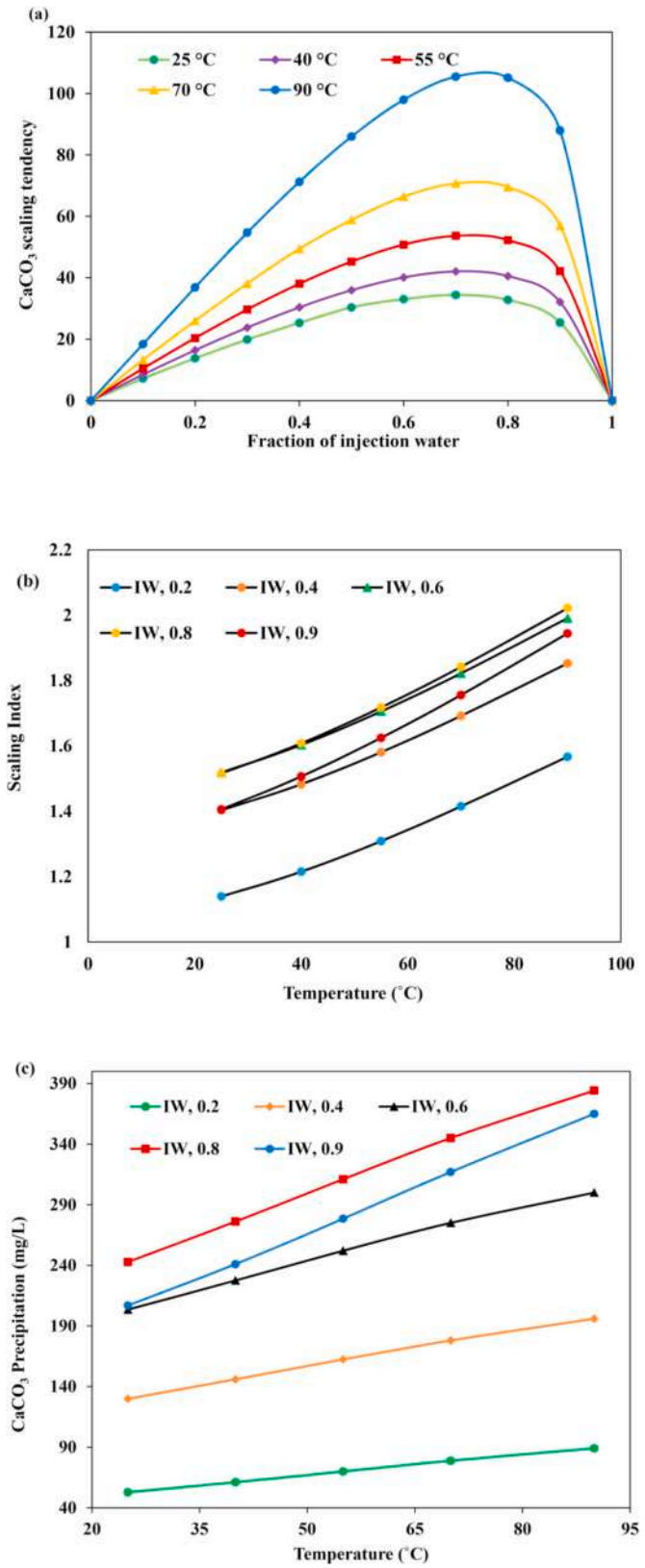

Fig. 4. a) The effect of temperature on the scaling tendency at the various fraction of IW, b) the effect of temperature on the scaling index under different IW fraction, c) the effect of temperature on the $CaCO_3$ precipitation at the various fraction of IW and atmospheric pressure.

CO_2, and having an elevated pH, than the injection water used is the cited study. It should be noted that the dissolution of $CaCO_3$ in the water is exothermic. Thus, an increase in the amount of the $CaCO_3$ deposition, scaling tendency, and scaling index of $CaCO_3$ by increasing temperature is associated with a reduction in solubility. As shown in Fig. 2, scale precipitation is directly linked to the increasing temperature. This observation is in good agreement with reported studies (Bahadori et al., 2010; Dyer and Graham, 2002; Khormali et al., 2016; MacAdam and Parsons, 2004; Moghadasi et al., 2003; Muryanto et al., 2014; Rousseau et al., 2003).

Fig. 5 illustrates the result of the influence of pressure and mixing ratio of brines on $CaCO_3$ scale deposition at a constant reservoir temperature of 90 °C. The amount of the $CaCO_3$ precipitation, scaling tendency, and scaling index of $CaCO_3$ formation were investigated at various pressure. The pressure range of 1–350 atm was selected for investigating the effect of reservoir pressure on the $CaCO_3$ precipitation during water flooding. As seen in this figure, increasing pressure slightly reduces the scaling tendency, reducing the $CaCO_3$ formation. For example, the predicted mass of $CaCO_3$ at 90 °C and 1, 150, 260, and 350 atm was about 249, 241, 235, and 230 mg/L of water, respectively, at the mixing ratio of 0.5:0.5 IW:FW. The dependence of $CaCO_3$ scale deposition on the pressure explains why the highest amount of this salt was formed at lower pressure. As pressure increased, the scaling tendency and scaling index of $CaCO_3$ was found to decrease. The reason for this behavior of $CaCO_3$ scale formation is that its solubility is increased slightly with an increase in pressure. The solubility of $CaCO_3$ is greatly influenced by the carbon dioxide content of the water, as the desorption of CO_2 causes an increase in pH and the degree of supersaturation of the carbonate solution. The effect becomes less pronounced as the temperature increases. As such, this is one of the major causes of $CaCO_3$ scale deposition on the walls of the production equipment (Dyer and Graham, 2002; Khormali et al., 2016; Wang et al., 2005; Zhang and Farquhar, 2001). The effect of temperature is more significant than that of pressure on $CaCO_3$ scaling tendency. Furthermore, Fig. 5c, as well as Fig. 4c, depict that the maximum amount of $CaCO_3$ formation occurred in a solution with a mixing of 0.8:0.2 IW:FW. Prediction software and static beaker tests provided beneficial information about the different conditions that $CaCO_3$ scale forms from a given quantity of mixture. However, these experiments were unable to describe extents and mechanisms of formation damage of the tight carbonate core samples during water injection processes due to scale formation. Therefore, the rate of $CaCO_3$ formation should be investigated during dynamic and core flood examinations.

3.2. *Induction time of $CaCO_3$ crystallization during dynamic flooding tests*

Turbidity is an indication of the inorganic salt deposition in the bulk solution and enables to determine the t_{ind} of $CaCO_3$ salt crystallization. The beginning of precipitation was detected by measuring the turbidity of the effluent sample after blending of two incompatible brines. Figs. 6 and 7 illustrate the turbidity measurement of calcium carbonate scale at 60 °C and 90 °C under a laminar flow regime. The flow rate of 1 ml/min was applied for the turbidity measurement in these tests. The procedure was taken at 15 min intervals for the first 90 min of salt precipitation, as shown in Figs. 6b and 7b, and later extended to every hundred minutes to capture the other stages of scale formation, as shown in Figs. 6a and 7a.

Due to the high ionic concentration of the brine solution, the nucleation mechanism for a high scaling tendency of 105 was fast as expected, which lead to less time induction period recorded. This result is in good agreement with observation reported in previous studies at high concentrations, which represent a fast precipitation of $CaCO_3$ salt (Chen et al., 2004, 2005a). It should be noted that the scaling tendency can be assumed constant during the experiments owing to their short residence time (6, 12, 24 min for 1, 0.5, and 0.25 ml/min, respectively).

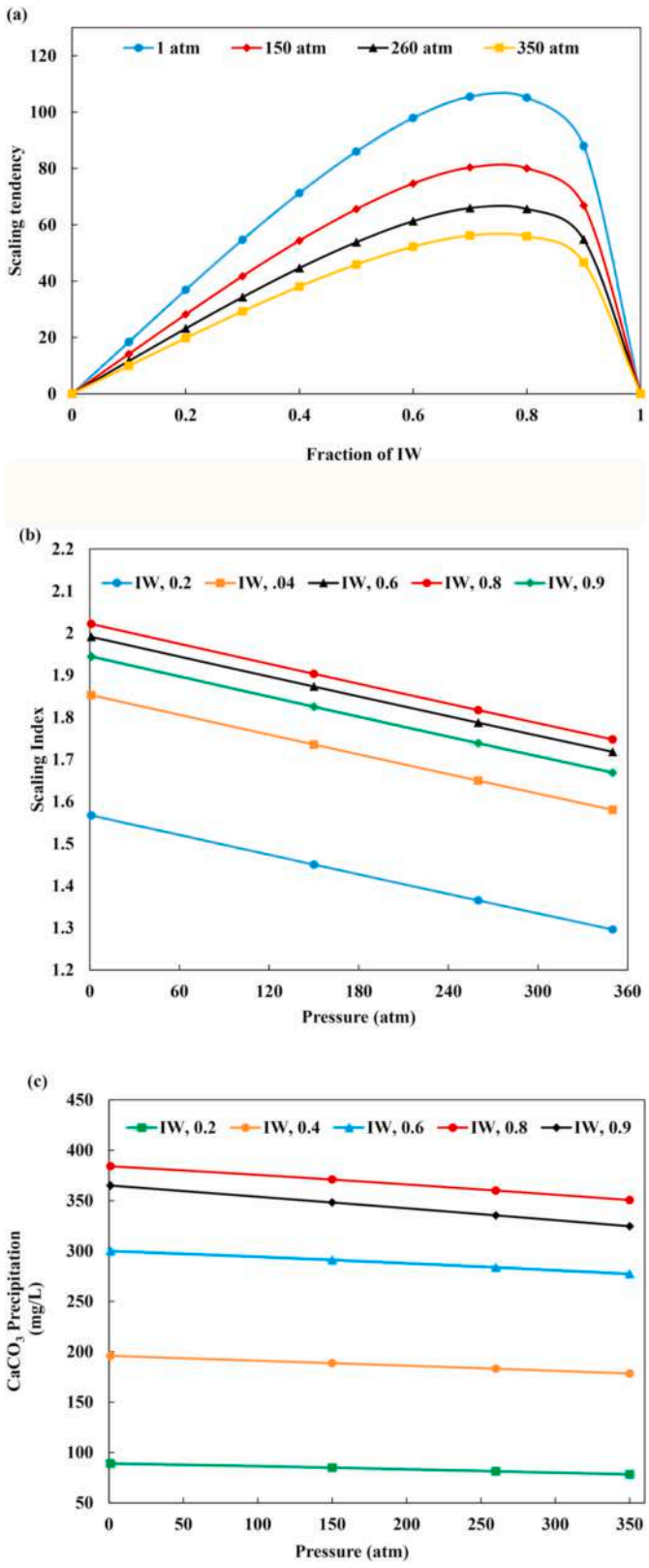

Fig. 5. a) The effect of pressure on the scaling tendency at various fractions of IW; b) the effect of pressure on the scaling index at various fractions of IW; c) the effect of pressure on the $CaCO_3$ precipitation at various fractions of IW.

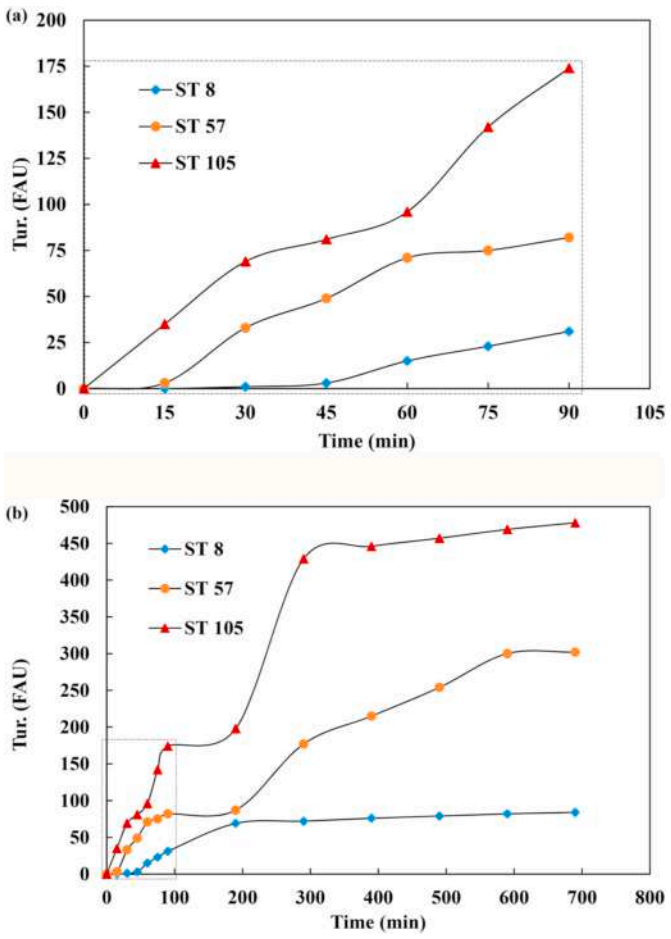

Fig. 6. Influence of ST on the turbidity versus time under a temperature of 60 °C and flow rate of 1 mL min^{-1}; (a) first 90 min of (b).

Residence time defines the time the fluid takes to travel through the capillary pipe after mixing and before it gets to the working section, which determined from Eq. (2):

$$\text{Residence time}(s) = \text{Volume of the system } (V)/\text{Injection rate}(Q) \quad (2)$$

Where V (mm^3) = $\pi r^2 l$, r indicates the internal radius of the capillary pipe (mm), and l denotes the length of the capillary pipe (mm).

For high scaling tendency, the induction period is less than the residence time. Therefore, there are crystals present in the effluent sample when incompatible fluids pass the capillary pipe, and the kinetic energy of the crystallization process is enhanced with increasing temperature due to the solubility of $CaCO_3$ decreases, as aforementioned. The precipitation rate for lower scaling tendencies was slow compared to the high scaling tendency. At 60 °C, induction times of 36 and 14 min were recorded for scaling tendencies of 8 and 57, respectively. Moreover, induction times of 22 and 9 min were obtained for scaling tendencies of 8 and 57 at 90 °C, respectively. Considering the results, it seems logical that the minimum amount of the crystals present in the effluent sample at a lower scaling tendency is owing to the induction period being greater than the residence time. As seen in the turbidity data, three different sections of the $CaCO_3$ crystallization process can be determined. A section with zero turbidity indicates the absence of precipitate in the effluent sample, which is referred to as the induction time. The next section sees the fast growth of $CaCO_3$ deposits, and in the subsequent section there is no additional deposition of scaling ions, which indicates the turbidity equilibrium or plateau region (Baraka-Lokmane and Hurtevent, 2012). Stamatakis et al. (2005) investigated the induction period of $CaCO_3$ deposition under dynamic flow

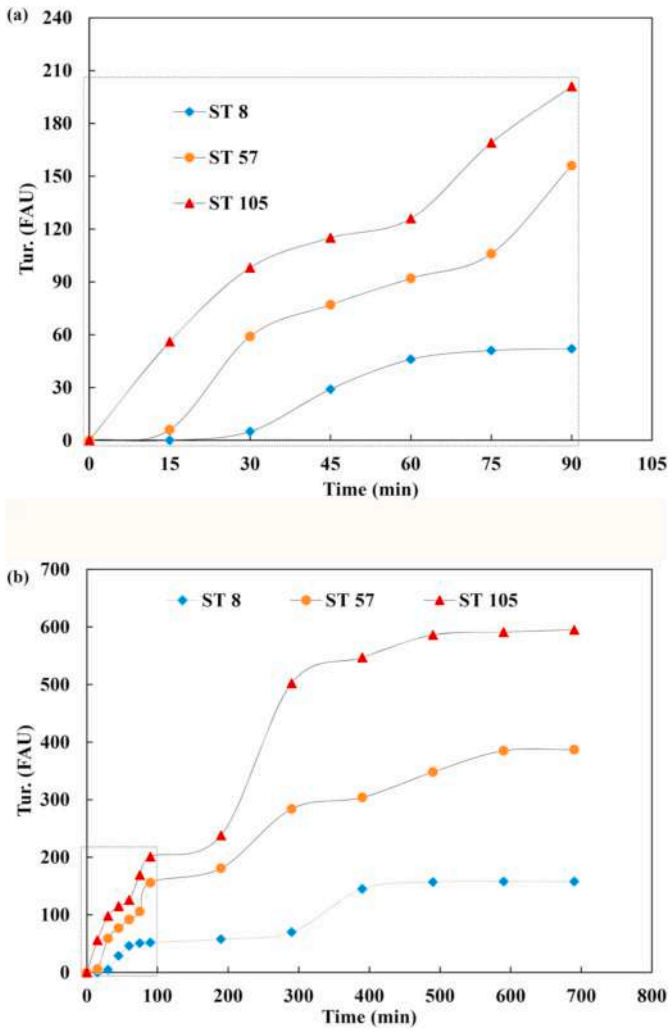

Fig. 7. Impact of ST on the turbidity versus time under a temperature of 90 °C and flow rate of 1 mL min^{-1}; a) first 90 min of (b).

conditions. Based on their results, the induction period is not related to the temperature at high scaling tendencies, and it depends on the primary degree of the solution scaling tendency. They stated that the crystal growth was controlled by the solution concentration at high-scaling tendencies.

The turbidity curves suggest two hypotheses with the brine composition studied. That is, a section where the low scaling tendency is dominated by the crystallization process, and a section where the high scaling tendency (i,e. ST = 105) where the scale mechanism is chiefly heterogeneous nucleation and adhesion. Crystal formation in the effluent sample was enhanced for the higher scaling tendency values. Also, the rate of $CaCO_3$ precipitation increased with temperature, which could increase the tendency for the scaling process through heterogeneous nucleation. There is a probability of the nucleation growth happening immediately as the highest amount of $CaCO_3$ inorganic deposition forms at the early stage of crystallization according to Setta et al. (2012). This indicates the formation of nuclei at the same time, which is followed by the growth of nuclei. Occasionally, small particles were seen at the beginning of experiments in the effluent sample. Some of these tiny particles turned out to be active sites during the experiments to grow the $CaCO_3$ scale owing to crystallization (Ramstad et al., 2005).

3.3. Extent of permeability reduction in tight carbonate core samples

Porous media is a complicated network of channels. Incompatible brine injection within such network channels is distinctly different from those existing in the capillary pipe and static beaker tests (Read and Ringen, 1982). The main goal of the core flooding tests is to determine the influence of mixing ratios, different low flow rates, temperature, and scaling tendency of injection brines on the permeability reduction of the tight carbonate core samples owing to $CaCO_3$ salt precipitation. In the first stage of permeability reduction investigation, mixing ratios of 0.7:0.3, 0.8:0.2 and 0.9:0.1 (IW:FW) in core flooding runs were examined. In Fig. 8, the effect of volume mixing ratio of incompatible brines on the permeability reduction of carbonate rocks at temperature of 90 °C and flow rate of 1 ml min^{-1} is shown. Based on this figure, at IW fraction of 0.8, degree of the permeability ratio is lower than that for IW fraction of 0.7 and 0.9. As a result, formation damage of the tight carbonate rocks in the ratio of 0.8:0.2 IW:FW is more than the other ratios. Core flooding examinations were performed in different low injection rates of 0.25, 0.5, and 1 ml/min with the working solution 0.8:0.2 IW:FW, at various scaling tendency of synthetic injection brines. Moreover, the experiments were carried out at two temperatures of 60 °C and 90 °C, which were reasonable for Iranian oil fields (Golkari and Riazi, 2018). Therefore, the core flooding tests were performed to estimate the worst formation damage (i.e. reduction in the rock permeability) at low flow rates due to $CaCO_3$ precipitation. No pressure was applied during these tests because pressure has an insignificant effect on the formation of $CaCO_3$ based on modeling results, which has already been explained in detail.

Real tight carbonate core samples were used to indicate the formation damage of the reservoir throughout the water injection process. Therefore, the reactions between the core samples and the injected brines are unavoidable. The rock permeability was measured by Darcy's linear flow equation. Damage to initial permeability (permeability reduction, K/K_i) was determined over time. The increase of the pressure drop or permeability reduction were indicators of the $CaCO_3$ scale formation in the rock samples.

3.3.1. The effect of low flow rate on formation damage of the rock samples

The fluid rate is a significant driving force for $CaCO_3$ forming in the rocks. To investigate the effect of low flow rates on the pressure drop and permeability reduction, a number of runs was carried out. Figs. 9 and 10 show the variation of pressure drop and permeability reduction as a function of time at different low flow injection rates. In these tests, the scaling tendency of injection brine and temperature were kept constant, and the flow rate changed. Fig. 10 illustrates that the permeability decline of core samples is evident, even at such low flow rates of 0.25

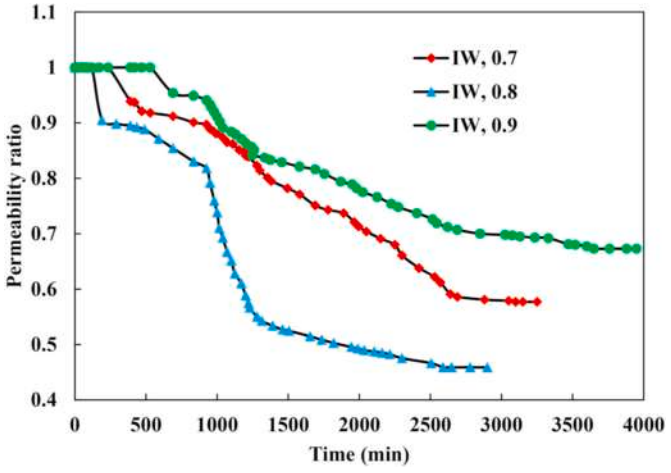

Fig. 8. The effect of volume mixing ratio on the permeability ratio at T = 90 °C and flow rate of 1 ml min^{-1}.

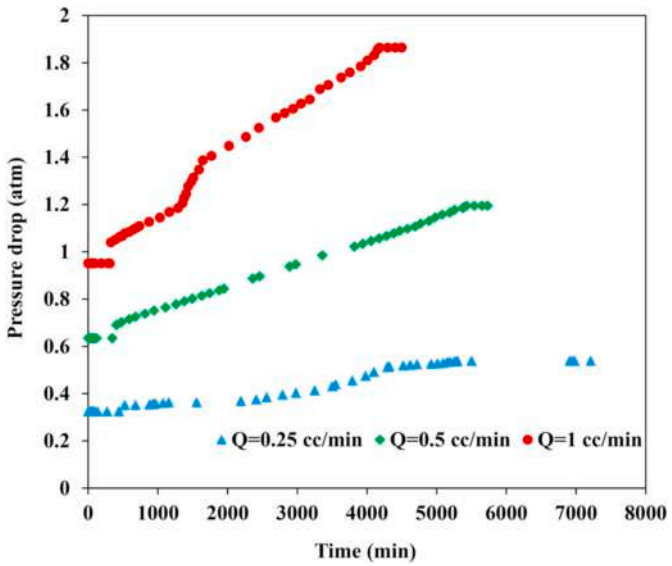

Fig. 9. Variation of pressure drop versus time for ST 57 at 90 °C.

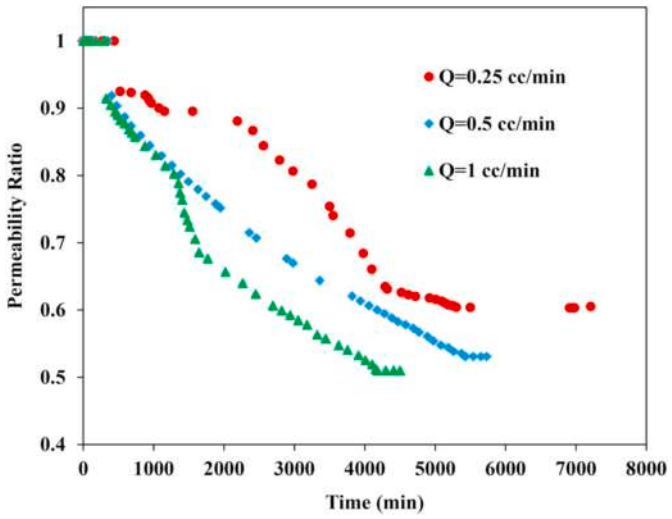

Fig. 10. Variation of permeability ratio versus time for ST 57 at 90 °C.

ml/min. The results show that at a low flow rate, $CaCO_3$ scale formation has a serious influence on permeability reduction. As the injection rate was increased, the permeability reduction becomes faster, and the rate of $CaCO_3$ deposition increases. At low flow rates of 0.25 ml/min for ST 57 at 90 °C, it took about 6910 min (115.16 h) for the permeability reduction to reach its maximum value. However, when the flow rate was increased to 0.5 and 1 ml/min, it took 5430 min (90.5 h) and 4180 min (69.66 h), respectively, to impose the overall damage on the core samples. This time in which the total damage occurred in the cores is called the deposition time. The kinetics of $CaCO_3$ scale formation were rapid as the deposition time decreased with the flow rate. In other words, at higher flow rates, more carbonate ions will pass through the cores in a given interval of time hence providing more substructure for $CaCO_3$ deposition. Based on the flow rates that were applied in these experiments, the permeability of the core samples decreased about 0.50 to 0.41 of the initial permeability.

3.3.2. *Effect of scaling tendency of mixed brines*

A series of runs were carried out to study the effect of different ionic concentrations in the IW and FW solutions on the permeability reduction of the cores owing to $CaCO_3$ formation. In these runs, the solution flow rate and temperature were kept constant at 0.5 ml/min and 60 °C, respectively, while using various three different brine concentrations (see Tables 4 and 5). Fig. 11 indicates the permeability decline trend variations with injection time when the core samples were injected with different solutions. In the solutions of a high degree of scaling tendency, super-saturation happened more quickly, leading to the permeability ratio declining more rapidly. The rate of $CaCO_3$ salt precipitation was rapid as the deposition time decreased with the scaling tendency. The greater formation damage of the cores due to $CaCO_3$ precipitation results from the presence of a significant concentration of calcium ion as compared to less formation damage occurring with lower content of calcium ion. This is expected, as an increase in supersaturation leads to a greater extent of scale precipitation rate, resulting in plugging of the pores. Due to these reasons, it is reasonable that as the scaling tendency decreases, $CaCO_3$ crystals become smaller. Therefore, the intensity of deposition and permeability reduction decreases.

3.3.3. *Effect of temperature on the formation damage of the cores*

To investigate the influence of temperature on the pressure drop and permeability reduction of the core plugs, a set of tests were performed. In these tests, the flow rate and scaling tendency of injection solution were kept constant, and the temperature varied from 60 to 90 °C. These experiments were carried out at a constant injection rate of 1 ml/min for mixed solution of ST 105. Typical results of pressure drop and permeability reduction with time at different temperatures are demonstrated in Fig. 12 and 13, respectively.

Fig. 13 shows that the permeability was reduced by 44% relative to the initial state (clean core plugs without any deposited scale) at a lower temperature (60 °C), while the permeability decreased by 54% relative to the initial state at an elevated temperature of 90 °C. The rate of precipitation and crystal growth was enhanced, so a considerable amount of $CaCO_3$ scales were deposited in carbonate core samples, and higher permeability reduction was detected. An increase in temperature causes a rise in super-saturation because the solubility of $CaCO_3$ decreases with temperature. Subsequently, the intensity of the scale deposition increases, and a faster permeability decline occurred. These results are in good agreement with the results of previous studies who admitted that the permeability reduction of porous media owing to $CaCO_3$ precipitation increases with rising temperature. The impact of temperature factor is evident for the formation of $CaCO_3$ deposits in some reservoirs with high-temperature conditions (Jordan et al., 2014; Moghadasi et al., 2003; Ramstad et al., 2005).

According to Fig. 12, as the temperature was increased, the pressure

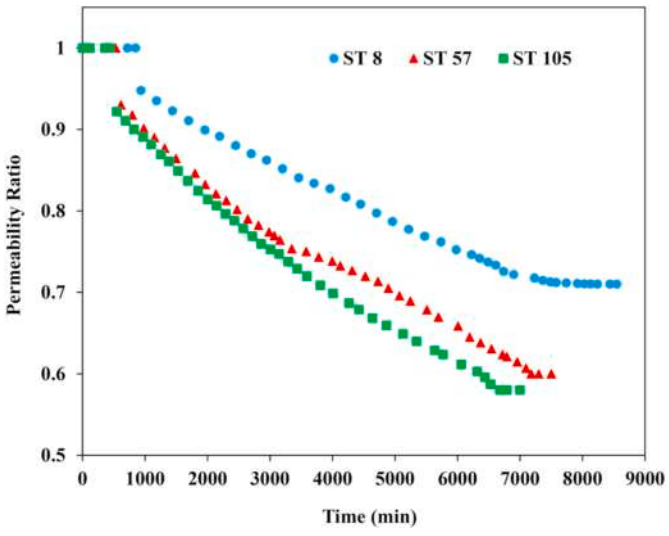

Fig. 11. Variation of permeability ratio versus time for the injection rate of 0.5 ml/min at 60 °C.

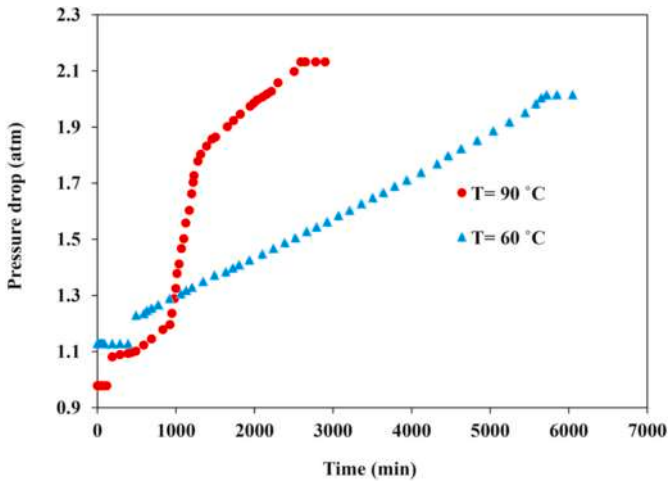

Fig. 12. Variation of pressure drop versus time at a constant injection rate of 1 ml/min for ST 105.

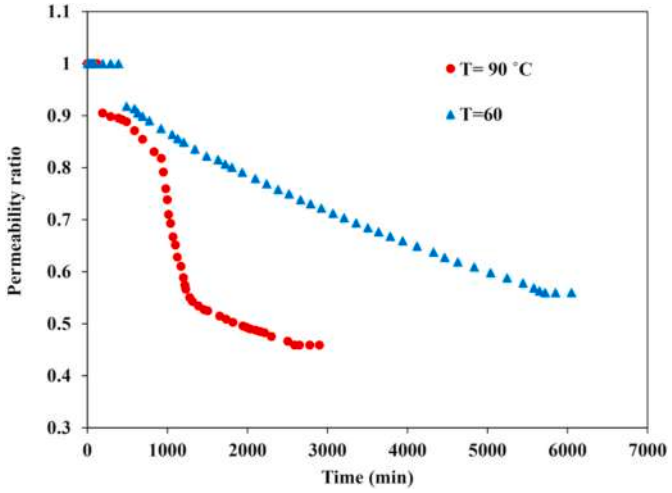

Fig. 13. Variation of permeability ratio versus time at a constant injection rate of 1 ml/min for ST 105.

drop along the core sample decreases more rapidly, which enhanced the deposition kinetics due to the rate of $CaCO_3$ deposition increases. In the case of 60 °C, the deposition time was 5720 min, compared to 90 °C, in which the deposition time of 2590 min was recorded. Moreover, at a temperature of 60 °C, it takes about 390 min for a pressure drop to become apparent, however, when the temperature is raised to 90 °C, it takes 120 min to impose the initial pressure drop on the cores. $CaCO_3$ nuclei are created more readily and they grow more quickly into particles at elevated temperatures (Dawe and Zhang, 1997; He et al., 1999). As the test fluids become hotter, more scale can form at the same time. This time in which the first formation damage manifested in the cores is denoted as the scaling period (t_s) and is analogous to the t_{ind} for turbidity measurement tests. This assumes that during the scaling period there is no crystal in the cores, since the beginning of the reduction of permeability remains the same. There is a fast decrease in permeability reduction that occurred after the scaling period, which is associated with accelerated nucleation and growth of $CaCO_3$ crystals in porous media. The scaling period before the start of the growth of nuclei was studied to predict the $CaCO_3$ scale risks in the cores.

The operating conditions used in these experiments and results of the permeability reduction tests are presented in Table 6. The correlation between scaling periods (t_s) and scaling tendencies (ST) provides a comprehensive understanding about the salt formation in the cores. Figs. 14 and 15 indicate the correlation between t_s and ST for 60 °C and 90 °C, respectively. It is clear that at various flow rates and temperatures the scaling tendency is inversely related to the scaling period (t_s). Decreased scaling tendency degree and flow rate increased the scaling period. A similar trend has been reported in literature (Mavredaki and Neville, 2014; Ramstad et al., 1999; Stamatakis et al., 2005).

Solution with a scaling tendency degree of 8 has the highest scaling period of 1030 min, while a solution with a scaling tendency degree of 105 has the lowest scaling period of 575 min for 0.25 ml/min and 60 °C as is depicted in Fig. 14. The long scaling period detected at lower scaling tendency results in low ionic strength of the injected solution as it passes through the cores, which reduces nucleation process speed. The formation of nuclei decreases due to a decrease in the mass transfer of calcium and bicarbonate ions in the injected solution. The movement of deposition ions in the injected solution determines the reaction rate or collision, which is faster at relatively higher flow rates of 0.5 and 1 ml/min, respectively.

In summary, it can be stated that the blockage of the cores increased rapidly with a flow rate at a greater degree of scaling tendency of mixed injection brines, resulting in a decrease in blocking time. It is in agreement with the work of researchers in which the scaling rate was a lot faster at higher saturation values and flow rates (Chen et al., 2005b; Moghadasi et al., 2003). The influence of high supersaturation on the

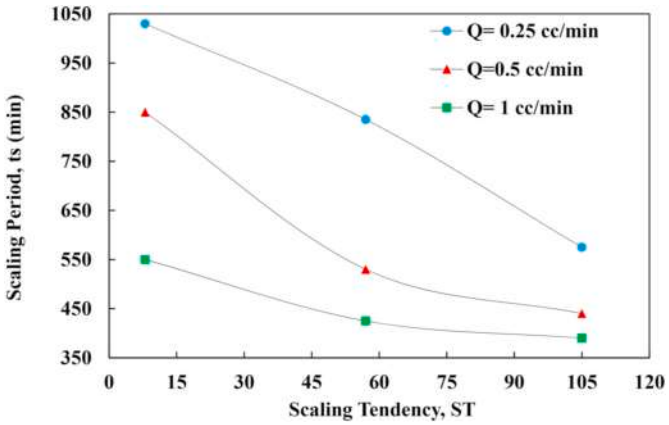

Fig. 14. Correlation between scaling period (t_s) and scaling tendency at 60 °C.

Table 6
List of the obtained results in core flooding tests at 60 °C and 90 °C.

Core number	1	2	3	4	5	6	7	8
Temperature (°C)	90	90	90	60	60	60	60	90
Flow rate (ml/min)	0.25	0.5	1	0.5	0.5	0.5	1	1
ST	57	57	57	8	57	105	105	105
Initial pressure drop (atm)	0.325	0.635	0.951	0.839	0.654	0.690	1.128	0.978
Final pressure drop (atm)	0.539	1.195	1.864	1.815	1.089	1.19	2.015	2.132
K/K_i	0.60	0.54	0.51	0.71	0.60	0.58	0.56	0.46
Scaling period (min)	440	345	310	850	530	440	390	120
Overall deposition time (min)	6910	5430	4180	8240	7180	6680	5720	2590

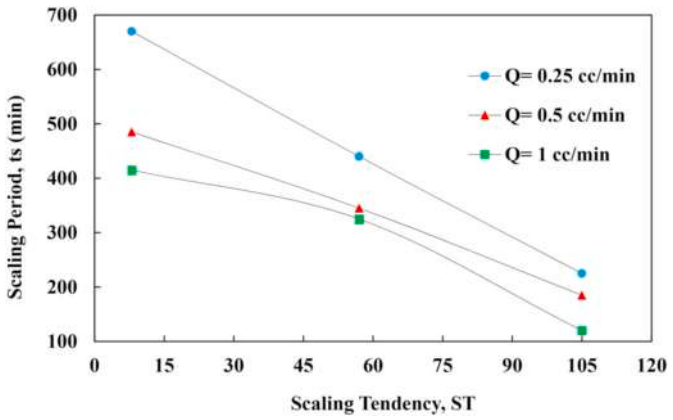

Fig. 15. Correlation between scaling period (t_s) and scaling tendency at 90 °C.

scale deposition kinetic is inevitable in this condition. Furthermore, the main reason for pore blockage possibly should be owing to heterogeneous nucleation (crystallization) and adhesion of pre-deposited scales as the kinetic mechanisms, which will be discussed later in detail. Also, the concentration of the scaling ions (calcium and bicarbonate) in the mixed injection brine has been considered as the main force of interaction (i.e. electric potential) of the deposit crystals for clogging the pore wall of the core samples (Israelachvili, 2011).

At a higher temperature of 90 °C, the nucleation process was faster than a lower temperature of 60 °C. Temperature increment lead to an increase in the reaction kinetics in the injected fluid, which in turn increases the rate of $CaCO_3$ formation in the cores, even at the similar scaling tendency degrees. A comparable trend was discovered for all scaling tendency degrees and injection flow rates examined in this study, in agreement with the turbidity measurement results. These results suggest that the formation damage of the tight carbonate core samples possibly results in $CaCO_3$ crystals blocking the pore throats. In all core flooding runs, the permeability decreased suddenly in the first minutes of injection. Furthermore, the curves in the figures subsequently reduced gradually as injection time continued. It illustrates that in every core flooding experiment, there was more inorganic deposits near the inlet part of the carbonate samples, while there was least $CaCO_3$ precipitation furthest from the inlet sections. In other words, the abundance of $CaCO_3$ scale decreased from the front of the core samples to the rear, demonstrating that $CaCO_3$ precipitation in the cores was fast due to permeability decreasing quickly after two incompatible brines were blended inside the tight carbonate cores. The examinations of deposit locations from the latest literature is in good agreement with the present work (Bedrikovetsky et al., 2005; Bin Merdhah, 2010; Jamialahmadi and Muller-Steinhagen, 2008; Todd and Yuan, 1992).

3.4. Heterogeneous nucleation (crystallization process) and adhesion processes in the core samples

Understanding the processes in which tight carbonate core samples blocking occurred and detecting the factors that affect the $CaCO_3$ deposition in the core samples help to establish a reliable predictive model for mechanisms of precipitation. The heterogeneous nucleation and adhesion process were quantitatively evaluated using induction time (i.e. scaling period). The scaling period before the start of growth nuclei is relying on the experimental method. The experimental investigation indicates that the procedure was well suited for $CaCO_3$ kinetics study, and a reduction in permeability was a useful method for studying $CaCO_3$ crystallization in the cores. However, it is occasionally difficult to obtain a correct calculation in core samples owing to its complexity. Additionally, the main external parameters, such as flow regime, interfacial tension, surface roughness, contact angle, and wettability, affect the crystallization and adhesion processes. This work focuses on tight Iranian carbonate core samples concerning to the flow rate, temperature, and scaling tendency of mixed injection brines at the ratio of 0.8:0.2 IW:FW, which are other important factors that influence the crystallization and adhesion processes (Holysz et al., 1994; H. Wang et al., 2013; Wang et al., 2005).

The precipitation of $CaCO_3$ scale on the pore walls of the cores can appear either by heterogeneous nucleation (crystallization) or adhesion of pre-precipitated inorganic deposits. These two hypotheses can simultaneously occur over a specific range of scaling tendencies of injection brines. $CaCO_3$ scale layer can be created by crystallization in the cores, where the crystals are exactly grown, and nucleated from the mixed brine scaling ions. The other principal mechanism by which the surface of rocks has an affinity with intermolecular forces, such as electrostatic forces, is the adhesion process. The $CaCO_3$ crystals can attach to the rock surface either by nucleated crystals being transported to the core samples or by agglomerating in the injection solution. Van der Waals force, chemical bonding, and electrostatic interaction are intermolecular forces that affect this process. Experimental conditions, nature of the crystals, and rock surface (substrate or the environment) have a significant impact on the adhesion of the $CaCO_3$ crystals to the pore wall of the rocks (Cheong et al., 2013; Israelachvili, 2011; Johnson, 1998; D. Packham and Johnston, 1994; D. E. Packham, 2006; Pedrosa et al., 2016). The heterogeneous nucleation process (crystallization process) and the interfacial energy of the $CaCO_3$ inorganic deposits to the pore wall of the core samples were determined from the correlation between $(\log ST)^2$ and $\log (t_s)$ (Bello, 2017; Mullin, 2001; Stamatakis et al., 2005).

$$Log\,(t_s) = A + \frac{B}{T^3(\log ST)^2} \tag{3}$$

$$B = V_m{}^2\,\beta\,f(\theta)\,N_A\,\gamma^3\ /\ (1.3\,R)^3 \tag{4}$$

where: V_m indicates the volume of one $CaCO_3$ unit ($6.132{\cdot}10^{-23}$ cm^3, calculated from the density and molar mass of calcite); β is a geometric factor of $\frac{16\pi}{3}$ for spherical shape crystal; f(θ) is a correction factor that is related to the type of nucleation; N_A indicates the Avogadro's constant (mol^{-1}); γ is the interfacial free energy or surface tension ($mJ{\cdot}m^{-2}$); R is the molar gas constant ($J{\cdot}mol^{-1}{\cdot}K^{-1}$); ST is the scaling tendency; t_s is the scaling period (s); A is dimensionless empirical constant; and T is the temperature (K).

From Eqs. (3) and (4), which are written based on the classical nucleation theory (Mullin, 2001), the main factors affecting the rate of nucleation are scaling tendency, temperature, and interfacial energy (i.e. surface energy). The relationship between these parameters could detect the boundary between heterogeneous nucleation (crystallization process) and adhesion processes in the cores that occurs within the injected solutions at a different range of scaling tendency. In other words, this boundary is based on the observation if the turbidity parameter of the mixing of injected brines was or was not increased sharply at the early stage of the tests. Figs. 16 and 17 indicate the crystallization processes in the tight carbonate cores at 60 °C and 90 °C, respectively, based on the relationship between $1/(\log ST)^2$ and $\log t_s$ for $CaCO_3$. According to the results obtained from these figures, the interfacial energy of the crystals to form in the cores was determined. Furthermore, scaling kinetic mechanisms to the pore wall of the cores were investigated during these examinations.

The right-hand section of Figs. 16 and 17 illustrate the lower scaling tendency degrees of 57 and 8. It can be seen that the scaling period of injected solutions with ST = 57 and ST = 8 were slow because they have low ionic strength. The heterogeneous nucleation (absolute crystallization) is the principal mechanism at a lower scaling tendency degree, which controls the risk of $CaCO_3$ precipitation during the core flooding processes as inferred from a linear correlation between $1/(\log ST)^2$ and $\log t_s$. This linear relationship between the scaling tendency and scaling period time is in good agreement with the results of Söhnel and Mullin

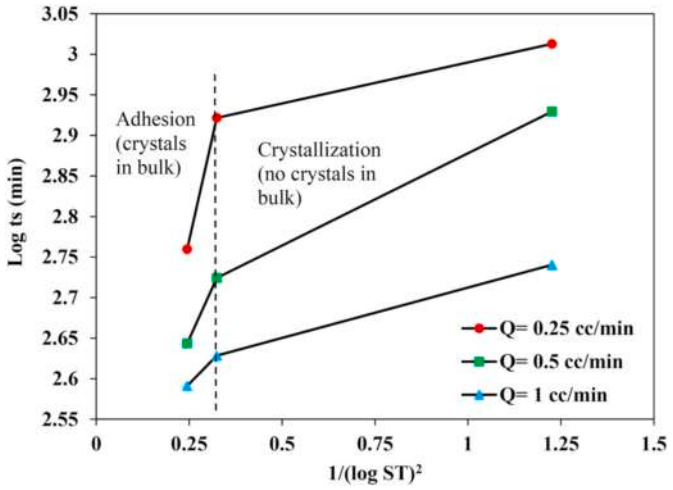

Fig. 16. Correlation between $1/(\log ST)^{2,}$ and log t_s at 60 °C.

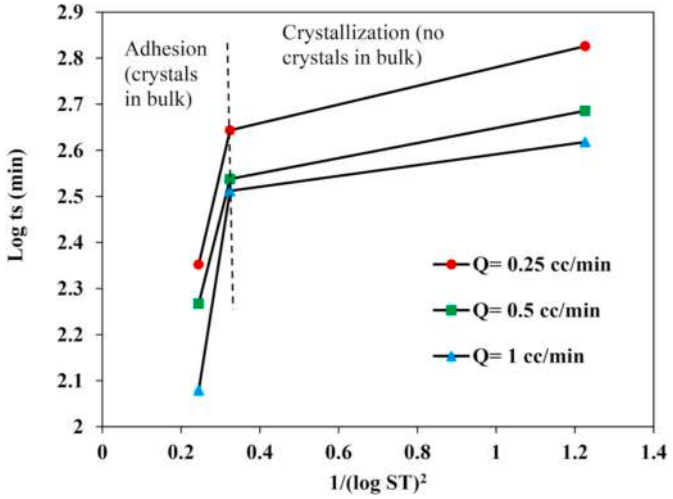

Fig. 17. Correlation between $1/(\log ST)^2$, and log t_s at 90 °C.

(1988). In their study, the diagram of $1/(\log ST)^2$ versus log t_s is divided into two regions, which individually have their own curved slope. Based on a level of scaling tendency in their work, two nucleation mechanisms were reported as homogeneous and heterogeneous nucleation.

In the present study, the diagram of $1/(\log ST)^2$ versus log t_s is divided into two regions, with the right-section indicating the crystallization mechanism (heterogeneous nucleation) and the left-section is generally a combination of adhesion and heterogeneous nucleation mechanisms. Furthermore, the same occurrences happened at 60 °C and 90 °C with the linear correlation between $1/(\log ST)^2$ and log t_s, which confirms the reports of other authors (Chien et al., 2007; Østvold and Randhol, 2001; Stamatakis et al., 2005) from the temperature increment point of view. These results are supported by turbidity measurement experiments, which were explained previously in detail. In this work, by the existence of the tight carbonate cores as a foreign substance, the nucleation mechanism is manifested better, and nucleation happened at the core nucleation sites.

The left-hand section of Figs. 16 and 17 display the higher scaling tendency degree of 105. It is expected that both heterogeneous nucleation and adhesion mechanisms are the causes of emerging $CaCO_3$ deposits in the cores through the core injection at ST = 105. In this case, the mechanism of $CaCO_3$ formation is controlled by nucleated crystals mobility or by agglomerated crystals depositing onto the pore wall of the cores where they adhere, causing permeability reduction in the tight carbonate core samples (Holysz et al., 1994; Kügler et al., 2016). As mentioned before, the $CaCO_3$ scale deposition rate was controlled by the flow rate, where deposition time was reduced with the increased injection rate in the cores. This examination could be due to the flow regime (creeping flow) in the range of low fluid injection rates used in this study.

Studies of Bazin et al. (2005), Chen et al. (2007) and Zhang and Farquhar (2001) reported that the scaling rate may be slow at a high flow rate, affecting the adherence of salt crystals to the substrate surface. Also, an investigation of Troup and Richardson (1978) showed that nucleation time decreased at a high flow rate because of the increment of nuclei formed on the substrate surface per unit area with an increased flow rate. It seems reasonable that increasing the injection rate did not have a great influence on the adherence of the $CaCO_3$ crystal to the pore wall of the cores. In other words, increased fluid injection rate leads to an increase in the mass transfer of the scaling ions, which in turn leads to the quick formation of $CaCO_3$ salts in the porous media.

3.5. Prediction of $CaCO_3$ scale deposition in tight carbonate cores based on the nucleation process

Prediction and determination of the parameters that influence the deposition of $CaCO_3$ in the carbonate core samples are an essential part of scale management in oilfield operations (Mackay et al., 2005). Various models of $CaCO_3$ scale prediction have been presented by various researchers (Bedrikovetsky et al., 2006; Haarberg et al., 1992; Østvold and Randhol, 2001; Stamatakis et al., 2005) for determining the probability of salt deposition. In these models, the emphasis is on the scaling tendency of the injected solution concerning the scaling period (t_s). The scaling period (t_s) in which the first permeability reduction appears in the cores is used as the key factor for the prediction model. The correlation between $1/(\log ST)^2$ and log t_s from Figs. 16 and 17 were examined and matched with the nucleation theory equation. Figs. 18 and 19, which were extracted from previous figures, illustrate the crystallization mechanism in the core samples due to $CaCO_3$ deposition, at 60 °C and 90 °C, respectively.

In the core flooding experimental setup designed in this work, the $CaCO_3$ crystals grow at the pore walls of the rocks, which are considered as an active site. The heterogeneous nucleation then occurs by a cluster unit of $CaCO_3$ at these active sites. The relationship between scaling period (t_s) and scaling tendency can be written by rearranging Eq. (3) as follows:

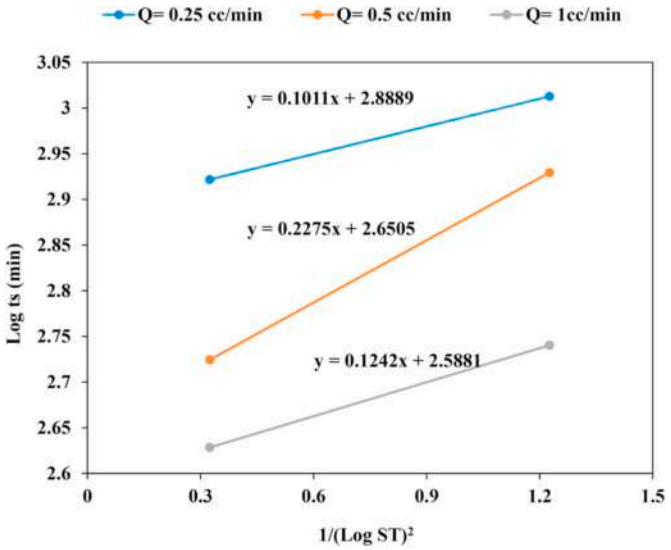

Fig. 18. Correlation between $1/(\log ST)^2$ and log t_s for crystallization mechanism at 60 °C.

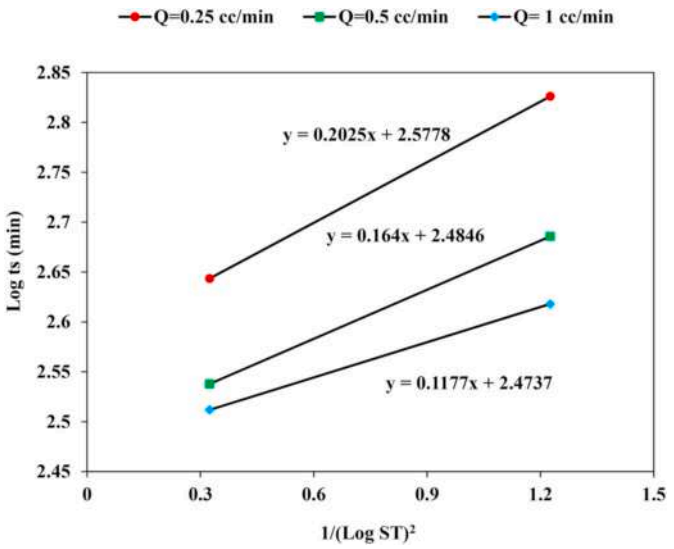

Fig. 19. Correlation between $1/(\log ST)^2$ and $\log t_s$ for crystallization mechanism at 90 °C.

$$Log\ (ts) = T^{-3}\, B(1/(\log ST))^2 + A \quad (5)$$

Tables 7 and 8 determine the main factors for interfacial energy (γ) and the nucleation hypothesis at different low flow rates for 60 °C and 90 °C, respectively. By determining the constants B and A from the slopes and intercepts of Figs. 18 and 19, the experimental correlation between $1/(\log ST)^2$ and $\log t_s$ were elucidated for tight carbonate core samples owing to $CaCO_3$ deposition.

Within the experimental correlations indicated in Eqs. 6-11 (Table 9), a semi-empirical model was achieved. The pore velocity values (flow rate/cross-sectional pore flow area) are indicated to ease comparison with other studies, and takes into account the mean core cross-sectional area and porosity used in this study (Table 3). It is the first step for providing a dependable approach to mitigate $CaCO_3$ salt in tight carbonate rocks under the mentioned conditions. Rock properties (initial porosity and permeability), flow conditions, and supersaturation values are essential factors in the prediction of scaling period and interfacial energy during the water flooding, and should be considered. The interfacial energy values determined from the core flooding tests are lower than what is reported in other works, owing to the examined substructures and techniques used in this study. According to the results of previous studies (Söhnel and Mullin, 1982; Spanos and Koutsoukos, 1998), heterogeneous nucleation mechanism manifested at low interfacial energy values. They also demonstrated that a high value of interfacial energy is due to unreasonable theory on data analysis.

4. Conclusions

In this study, beaker tests and OLI Scale Chem and ScaleSoftPitzer software were used for $CaCO_3$ precipitation prediction under static conditions. For investigating the mechanisms of $CaCO_3$ formation in tight carbonate rocks, turbidity measurement techniques, and carbonate core flooding tests under dynamic conditions were examined. According to the results achieved from this work, the following conclusions can be drawn:

Table 7
Crystallization factors according to heterogeneous nucleation hypothesis values at 60 °C.

Injection rate, mL/min	A	B	Interfacial energy (mJ/m^2)
0.25	2.8889	$3.75{\cdot}10^6$	0.02504
0.5	2.6505	$8.4{\cdot}10^6$	0.03276
1	2.5881	$4.58{\cdot}10^6$	0.02676

Table 8
Crystallization factors according to heterogeneous nucleation hypothesis values at 90 °C.

Injection rate, mL/min	A	B	Interfacial energy (mJ/m^2)
0.25	2.5778	$9.69{\cdot}10^6$	0.04113
0.5	2.4846	$7.84{\cdot}10^6$	0.03832
1	2.4737	$5.63{\cdot}10^6$	0.03432

Table 9
The experimental correlation of $CaCO_3$ deposition.

Injection rate (ml/min)	Pore velocity (cm/min)	T (K)	Correlation (T in Kelvin)	Equation
0.25	0.178	333	$\log(t_s) = T^{-3} \cdot 3.75{\cdot}10^6 \cdot (1/(\log ST)^2) + 2.8889$	6
0.25	0.178	363	$\log(t_s) = T^{-3} \cdot 9.69{\cdot}10^6 \cdot (1/(\log ST)^2) + 2.5778$	7
0.5	0.356	333	$\log(t_s) = T^{-3} \cdot 8.40{\cdot}10^6 \cdot (1/(\log ST)^2) + 2.6505$	8
0.5	0.356	363	$\log(t_s) = T^{-3} \cdot 7.84{\cdot}10^6 \cdot (1/(\log ST)^2) + 2.4846$	9
1	0.712	333	$\log(t_s) = T^{-3} \cdot 4.58{\cdot}10^6 \cdot (1/(\log ST)^2) + 2.5881$	10
1	0.712	363	$\log(t_s) = T^{-3} \cdot 5.63{\cdot}10^6 \cdot (1/(\log ST)^2) + 2.4737$	11

1) The maximum amount of $CaCO_3$ salt was precipitated in the solution with a volume mixing ratio of 0.8:0.2 IW:FW at a temperature of 90 °C. Therefore, the worst $CaCO_3$ scale scenario at 80% IW in the working solution could lead to high permeability loss and severe formation damage in the rock samples.
2) The predicted results using the OLI software and the measured actual mass of the deposition using the beaker tests were in agreement. In addition, the discrepancy of the beaker test and OLI prediction results on the amount of $CaCO_3$ salt (mg/l) was less than 3%, while the error using the ScaleSoftPitzer program was about 8%.
3) At low scaling tendency of 8 and 57, the induction period reported illustrates that there will be no crystals in the bulk solution as it moves through the capillary pipe. At a high scaling tendency of 105, there is no induction period reported, hence $CaCO_3$ deposition is prone to be controlled by a mixed mechanism of adhesion and heterogeneous nucleation.
4) The intensity of permeability reduction of tight carbonate core samples due to $CaCO_3$ salt was investigated using 0.8:0.2 IW:FW. As this proportion gives the highest amount of $CaCO_3$ solid based on the static tests, it was selected to examine the mechanisms of severe formation damage in the rock samples.
5) Examination of the effect of different low flow rates of 0.25, 0.5, and 1 ml/min (0.178–0.712 cm/min pore velocities) on $CaCO_3$ precipitation kinetic in the core samples indicates that the adherence of scale to the pore wall of the cores is dependent on low injection rates.
6) At various flow rates and temperatures, the scaling tendency is inversely related to the scaling period (t_s). Decreased scaling tendency degree and flow rate increased the scaling period. The long scaling period detected at lower scaling tendency results in low ionic strength of the injected solution as it passes through the cores, which reduces nucleation kinetics.
7) The nucleation mechanism was fast at a high degree of scaling tendency of 105, and a short scaling period (t_s) was recorded at this degree of scaling tendency. Increasing deposition time and scaling period (t_s) was observed at a low degree of scaling tendencies or low concentration of deposition ions in the mixed injection brines.
8) The diagram of $1/(\log ST)^2$ versus $\log t_s$ is divided into two regions indicates that two inorganic deposit processes within the scaling tendencies examined. At low scaling tendencies, crystallization

mechanism control $CaCO_3$ scale deposition, while at higher scaling tendencies, heterogeneous nucleation and adhesion processes occurred in carbonate rocks. This scenario is supported by turbidity measurement tests.

9) The surface energies obtained from the semi-empirical modeling study are low compared to those that were achieved from the other works of literature. This difference is related to the experimental condition in this work. However, it should be mention other studies have stated that heterogeneous nucleation mechanisms take place at low surface energy, which is in agreement with this study.

Credit author statement

Sajjad Qazvini: Writing – original draft, Investigation, Resources, Abdolah Golkari: Methodology, Funding acquisition, Writing – review & editing. Amin Azdarpour: Methodology, Validation, Resources, Data curation, Supervision, Project administration, Funding acquisition, Writing – review & editing, Rafael M. Santos: Writing – review & editing. Mir Saeid Safavi: Methodology, Funding acquisition, Writing – review & editing. Milad Norouzpour: Resources, Funding acquisition, Writing – review & editing

Declaration of competing interest

The authors declare that they have no known competing financial interests or personal relationships that could have appeared to influence the work reported in this paper.

Acknowledgement

The authors would like to gratefully acknowledge and show appreciation to the Department of Petroleum Engineering, Faculty of Engineering, Marvdasht Islamic Azad University, Marvdasht, Iran for the provision of the laboratory facilities necessary for completing this work.

List of symbols

IW	Injection Water
FW	Formation water
$CaCO_3$	Calcium carbonate
$CaSO_4$	Calcium sulfate
$BaSO_4$	Barium sulfate
$SrSO_4$	Strontium sulfate
ST	Scaling tendency
SI	Scaling index
t_{ind}	Bulk induction time (s)
t_s	Scaling period (s)
K_{sp}	Solubility product constant of $CaCO_3$ (mol^2/L^2)
HCl	Hydrochloric acid
NaOH	Sodium hydroxide
Na_2CO_3	Sodium carbonate
KOH	Potassium hydroxide
HEDTA	Hydroxyethyl ethylene diamine tetra acetic acid
EDTA	Ethylene diamine tetra acetic acid
T	Temperature (°C or K)

References

Abdel-Aal, N., Satoh, K., Sawada, K., 2002. Study of the adhesion mechanism of $CaCO_3$ using a combined bulk chemistry/QCM technique. J. Cryst. Growth 245 (1–2), 87–100.

Al-Roomi, Y.M., Hussain, K.F., Al-Rifaie, M., 2015. Performance of inhibitors on $CaCO_3$ scale deposition in stainless steel & copper pipe surface. Desalination 375, 138–148.

Al Tolaihy, M., Bukhari, D.O., Wu, A.M., 2010. Study on the optimization of de-scaling operations in Saudi arabian khuff gas wells. In: Paper Presented at the CORROSION 2010.

Almubarak, T., Ng, J.H., Nasr-El-Din, H., 2017. Oilfield scale removal by chelating agents: an aminopolycarboxylic acids review. In: Paper Presented at the SPE Western Regional Meeting.

Amiri, M., Moghadasi, J., Jamialahmadi, M., 2013. Prediction of iron carbonate scale formation in Iranian oilfields at different mixing ratio of injection water with formation water, energy sources, Part A: recovery, utilization. and Environmental Effects 35 (13), 1256–1265.

Aqrawi, A.A., Goff, J.C., Horbury, A.D., Sadooni, F.N., 2010. The Petroleum Geology of Iraq. Scientific press.

Aziz, B., Gebauer, D., Hedin, N., 2011. Kinetic control of particle-mediated calcium carbonate crystallization. CrystEngComm 13 (14), 4641–4645.

Bageri, B., Mahmoud, M., Shawabkeh, R.A., Al-Mutairi, S., Abdulraheem, A., 2017. Toward a complete removal of barite (barium sulfate $$\hbox {BaSO} _ {4} $$) scale using chelating agents and catalysts. Arabian J. Sci. Eng. 42 (4), 1667–1674.

Bahadori, A., Vuthaluru, H., Ang, M., 2010. Predictive tool for estimation of potential precipitation from an equilibrated calcium carbonate aqueous phase. In: Paper Presented at the Trinidad and Tobago Energy Resources Conference.

Baraka-Lokmane, S., Hurtevent, C., 2012. Chemical incompatibilities between formation water and injection sea water; comparison between modeling and site observations in fields operated by TOTAL. In: Paper Presented at the Abu Dhabi International Petroleum Conference and Exhibition.

Bazin, B., Kohler, N., Zaitoun, A., 2005. Some insights into the tube-blocking-test method to evaluate the efficiency of mineral scale inhibitors. In: Paper Presented at the SPE Annual Technical Conference and Exhibition.

Bedrikovetsky, P., Mackay, E., Moraes, G., Rosario, F., Monteiro, R., 2006. Laboratory-based prediction of sulphate scaling damage. In: Paper Presented at the SPE International Oilfield Scale Symposium.

Bedrikovetsky, P., Moraes, G., Monteiro, R., Lopes, R., Rosario, F., Bezerra, M., 2005. Characterization of sulphate scaling formation damage from laboratory measurements (to predict well-productivity decline). In: Paper Presented at the SPE International Symposium on Oilfield Chemistry.

Bello, O., 2017. Calcium Carbonate Scale Deposition Kinetics on Stainless Steel Surfaces. University of Leeds.

Bin Merdhah, A., 2010. Inhibition of calcium sulfate and strontium sulfate scale in waterflood. SPE Prod. Oper. 25 (4), 545–552, 0.

BinMerdhah, A.B., Yassin, A.A.M., Muherei, M.A., 2010. Laboratory and prediction of barium sulfate scaling at high-barium formation water. J. Petrol. Sci. Eng. 70 (1–2), 79–88.

Birol, F., Cozzi, L., Gould, T., Bromhead, A., Priddle, R., 2015. World outlook energy. World Energy Outlook 1–12, 2015.

Chen, T., Neville, A., Sorbie, K., Zhong, Z., 2007. In-situ monitoring the inhibiting effect of detpmp on Caco3 scale formation by synchrotronx-ray diffraction. In: Paper Presented at the CORROSION 2007.

Chen, T., Neville, A., Yuan, M., 2004. Influence of Mg2+ on the kinetics and crystal morphology of CaCO3 scale formation on the metal surface and in bulk solution. In: Paper Presented at the CORROSION 2004.

Chen, T., Neville, A., Yuan, M., 2005a. Assessing the effect of Mg2+ on CaCO3 scale formation–bulk precipitation and surface deposition. J. Cryst. Growth 275 (1–2), e1341–e1347.

Chen, T., Neville, A., Yuan, M., 2005b. Calcium carbonate scale formation—assessing the initial stages of precipitation and deposition. J. Petrol. Sci. Eng. 46 (3), 185–194.

Cheong, W., Gaskell, P., Neville, A., 2013. Substrate effect on surface adhesion/crystallisation of calcium carbonate. J. Cryst. Growth 363, 7–21.

Chibowski, E., Hołysz, L., Terpiłowski, K., 2003. Effect of magnetic field on deposition and adhesion of calcium carbonate particles on different substrates. J. Adhes. Sci. Technol. 17 (15), 2005–2021.

Chien, W.-C., Lee, C.-C., Tai, C.Y., 2007. Heterogeneous nucleation rate of calcium carbonate derived from induction period. Ind. Eng. Chem. Res. 46 (20), 6435–6441.

Dawe, R.A., Zhang, Y., 1997. Kinetics of calcium carbonate scaling using observations from glass micromodels. J. Petrol. Sci. Eng. 18 (3–4), 179–187.

Duggirala, P.Y., 2005. Formation of calcium carbonate scale and control strategies in continuous digesters, CD del II Coloquio Internacional sobre Celulosa de Eucalipto, Concepción, Chile. Mayo.

Dyer, S.J., Graham, G.M., 2002. The effect of temperature and pressure on oilfield scale formation. J. Petrol. Sci. Eng. 35 (1–2), 95–107.

Golkari, A., Riazi, M., 2018. Comparative study of oil spreading characteristics for water and carbonated water systems using live and dead oils. J. Petrol. Sci. Eng. 171, 242–252.

Haarberg, T., Selm, I., Granbakken, D.B., Ostvold, T., Read, P., Schmidt, T., 1992. Scale formation in reservoir and production equipment during oil recovery: an equilibrium model. SPE Prod. Eng. 7 (1), 75–84, 0.

Haghtalab, A., Kamali, M., Shahrabadi, A., Golghanddashti, H., 2015. Investigation of the precipitation of calcium sulfate in porous media: experimental and mathematical modeling. Chem. Eng. Commun. 202 (9), 1221–1230.

Hall, B., Dill, W., 1988. Iron control additives for limestone and sandstone acidizing of sweet and sour wells. In: Paper Presented at the SPE Formation Damage Control Symposium.

He, S., Kan, A.T., Tomson, M.B., 1999. Inhibition of calcium carbonate precipitation in NaCl brines from 25 to 90 C. Appl. Geochem. 14 (1), 17–25.

Holysz, L., Chibowski, E., Wójcik, W., Busch, K.W., Busch, M.A., 1994. Parameters determining the deposition of calcium carbonate into a glass capillary. J. Adhes. Sci. Technol. 8 (2), 181–193.

Israelachvili, J.N., 2011. Intermolecular and Surface Forces. Academic press.

Jamialahmadi, M., Muller-Steinhagen, H., 2008. Mechanisms of scale deposition and scale removal in porous media. Int. J. Oil Gas Coal Technol. 1 (1–2), 81–108.

Johnson, K., 1998. Mechanics of adhesion. Tribol. Int. 31 (8), 413–418.

Jordan, M.M., Williams, H., Linares-Samaniego, S., Frigo, D.M., 2014. New insights on the impact of high temperature conditions (176 C) on carbonate and sulphate scale dissolver performance. In: Paper Presented at the SPE International Oilfield Scale Conference and Exhibition.
Kamal, M.S., Hussein, I., Mahmoud, M., Sultan, A.S., Saad, M.A., 2018. Oilfield scale formation and chemical removal: a review. J. Petrol. Sci. Eng. 171, 127–139.
Kamari, A., Gharagheizi, F., Bahadori, A., Mohammadi, A.H., 2014. Determination of the equilibrated calcium carbonate (calcite) scaling in aqueous phase using a reliable approach. Journal of the Taiwan Institute of Chemical Engineers 45 (4), 1307–1313.
Kan, A., Tomson, M., 2012. Scale prediction for oil and gas production. SPE J. 17 (2), 362–378, 0.
Kelland, M.A., 2014. Production Chemicals for the Oil and Gas Industry. CRC press.
Khormali, A., Petrakov, D.G., Lamidi, A.-L.B., Rastegar, R., 2015. Prevention of calcium carbonate precipitation during water injection into high-pressure high-temperature wells. In: Paper Presented at the SPE European Formation Damage Conference and Exhibition.
Khormali, A., Petrakov, D.G., Moein, M.J.A., 2016. Experimental analysis of calcium carbonate scale formation and inhibition in waterflooding of carbonate reservoirs. J. Petrol. Sci. Eng. 147, 843–850.
Kiaei, Z., Haghtalab, A., 2014. Experimental study of using Ca-DTPMP nanoparticles in inhibition of CaCO3 scaling in a bulk water process. Desalination 338, 84–92.
Kügler, R.T., Beißert, K., Kind, M., 2016. On heterogeneous nucleation during the precipitation of barium sulfate. Chem. Eng. Res. Des. 114, 30–38.
Lawler, D., 2016. Turbidity, Turbidimetry, and Nephelometry Chemistry, Molecular Sciences and Chemical Engineering. Elsevier, pp. 1–2.
LePage, J.N., De Wolf, C., Bemelaar, J., Nasr-El-Din, H.A., 2009. An environmentally friendly stimulation fluid for high-temperature applications. In: Paper Presented at the SPE International Symposium on Oilfield Chemistry.
Li, J., Tang, M., Ye, Z., Chen, L., Zhou, Y., 2017. Scale formation and control in oil and gas fields: a review. J. Dispersion Sci. Technol. 38 (5), 661–670.
Liu, X., Chen, T., Chen, P., Montgomerie, H., Hagen, T.H., Wang, B., Yang, X., 2012. Understanding mechanisms of scale inhibition using newly developed test method and developing synergistic combined scale inhibitors. In: Paper Presented at the SPE International Conference on Oilfield Scale.
Liu, Y., Kan, A., Zhang, Z., Yan, C., Yan, F., Zhang, F., Bhandari, N., Dai, Z., Ruan, G., Wang, L., 2016. An assay method to determine mineral scale inhibitor efficiency in produced water. J. Petrol. Sci. Eng. 143, 103–112.
Lu, H., Kan, A.T., Zhang, P., Yu, J., Fan, C., Tomson, M.B., 2010. Phase stability and solubility of calcium sulfate in the system NaCl/monoethylene glycol/water. In: Paper Presented at the SPE International Conference on Oilfield Scale.
MacAdam, J., Parsons, S.A., 2004. Calcium carbonate scale formation and control. Rev. Environ. Sci. Biotechnol. 3 (2), 159–169.
Mackay, E.J., Collins, I., Jordan, M., Feasey, N.P.W.R.I., 2003. Scale formation risk assessment and management. In: Paper Presented at the International Symposium on Oilfield Scale.
Mackay, E.J., Jordan, M.M., 2005. Impact of Brine Flow and Mixing in the Reservoir on Scale Control Risk Assessment and Subsurface Treatment Options: Case Histories.
Mackay, E.J., Jordan, M.M., Feasey, N.D., Shah, D.J., Kumar, P.S., Ali, S.A., 2005. Integrated risk analysis for scale management in deepwater developments. SPE Prod. Facil. 20 (2), 138–154, 0.
Mavredaki, E., Neville, A., 2014. Prediction and evaluation of calcium carbonate deposition at surfaces. In: Paper Presented at the SPE International Oilfield Scale Conference and Exhibition.
Merdhah, A., 2010. Inhibition of calcium sulfate and strontium sulfate scale in waterflood. SPE Prod. Oper. 25 (4), 545–552. https://doi.org/10.2118/141168-PA. SPE-141168-PA.
Mitrouli, S., Kostoglou, M., Karabelas, A., 2016. Calcium carbonate scaling of desalination membranes: assessment of scaling parameters from dead-end filtration experiments. J. Membr. Sci. 510, 293–305.
Moghadasi, J., Jamialahmadi, M., Müller-Steinhagen, H., Sharif, A., 2004a. Formation damage due to scale formation in porous media resulting from water injection. In: Paper Presented at the SPE International Symposium and Exhibition on Formation Damage Control.
Moghadasi, J., Jamialahmadi, M., Müller-Steinhagen, H., Sharif, A., Ghalambor, A., Izadpanah, M., Motaie, E., 2003. Scale formation in Iranian oil reservoir and production equipment during water injection. In: Paper Presented at the International Symposium on Oilfield Scale.
Moghadasi, J., Müller-Steinhagen, H., Jamialahmadi, M., Sharif, A., 2004b. Model study on the kinetics of oil field formation damage due to salt precipitation from injection. J. Petrol. Sci. Eng. 43 (3–4), 201–217.
Mullin, J.W., 2001. Crystallization. Elsevier.
Muryanto, S., Bayuseno, A., Ma'Mun, H., Usamah, M., 2014. Calcium carbonate scale formation in pipes: effect of flow rates, temperature, and malic acid as additives on the mass and morphology of the scale. Procedia Chemistry 9, 69–76.
Nergaard, M., Grimholt, C., 2010. An Introduction to Scaling Causes, Problems and Solutions, Term Paper for the Course TPG.
Olajire, A.A., 2015. A review of oilfield scale management technology for oil and gas production. J. Petrol. Sci. Eng. 135, 723–737.
Østvold, T., Randhol, P., 2001. Kinetics of CaCO3 scale formation. The influence of temperature, supersaturation and ionic composition. In: Paper Presented at the International Symposium on Oilfield Scale.
Packham, D., Johnston, C., 1994. Mechanical adhesion: were McBain and Hopkins right? An empirical study. Int. J. Adhesion Adhes. 14 (2), 131–135.
Packham, D.E., 2006. Handbook of Adhesion. John Wiley & Sons.
Pedrosa, J., Gamelas, J., Lourenço, A.F., Ferreira, P.J., 2016. Surface Properties of Calcium Carbonate Modified with Silica by Sol-Gel Method A Physicochemical and Engineering Aspects.
Ramstad, K., Tydal, T., Askvik, K.M., Fotland, P., 2005. Predicting carbonate scale in oil producers from high temperature reservoirs. SPE J. 10 (4), 363–373, 0.
Ramstad, K., Tydal, T., Ellersten, E., Jakobsen, T., 1999. Precipitation and deposition of CaCO3. Laboratory studies and field experience. In: Paper Presented at the NIF Tenth International Oil Field Chemicals Symposium. Fagernes, Norway, Mar.
Rashid, F., Glover, P., Lorinczi, P., Collier, R., Lawrence, J., 2015. Porosity and permeability of tight carbonate reservoir rocks in the north of Iraq. J. Petrol. Sci. Eng. 133, 147–161.
Read, P.A., Ringen, J.K., 1982. The use of laboratory tests to evaluate scaling problems during water injection. In: Paper Presented at the SPE Oilfield and Geothermal Chemistry Symposium.
Rousseau, G., Hurtevent, C., Azaroual, M., Kervevan, C., Durance, M.-V., 2003. Application of a thermo-kinetic model to the prediction of scale in Angola block 3 field. In: Paper Presented at the International Symposium on Oilfield Scale.
ScaleSoftPitzer, 2009. ScaleSoftPitzer™(Version 13.0). Energy & Environmental Systems Institute, Rice University, Houston TX77005. Rice University Brine Chemistry Consortium.
Setta, F.-A., Neville, A., Chen, H.J., 2012. A surface kinetic scaling model for CaCO 3 on a stainless steel surface (316 L). In: Paper Presented at the CORROSION 2012.
Shokrollahi, A., Safari, H., Esmaeili-Jaghdan, Z., Ghazanfari, M.H., Mohammadi, A.H., 2015. Rigorous modeling of permeability impairment due to inorganic scale deposition in porous media. J. Petrol. Sci. Eng. 130, 26–36.
Söhnel, O., Mullin, J., 1982. Precipitation of calcium carbonate. J. Cryst. Growth 60 (2), 239–250.
Söhnel, O., Mullin, J., 1988. Interpretation of crystallization induction periods. J. Colloid Interface Sci. 123 (1), 43–50.
Sousa, M.F., Signorelli, F., Bertran, C.A., 2016. Fast evaluation of inhibitors for calcium carbonate scale based on pH continuous measurements in jar test at high salinity condition. J. Petrol. Sci. Eng. 147, 468–473.
Spanos, N., Koutsoukos, P.G., 1998. Kinetics of precipitation of calcium carbonate in alkaline pH at constant supersaturation. Spontaneous and seeded growth. J. Phys. Chem. B 102 (34), 6679–6684.
Stamatakis, E., Stubos, A., Palyvos, J., Chatzichristos, C., Muller, J., 2005. An improved predictive correlation for the induction time of CaCO3 scale formation during flow in porous media. J. Colloid Interface Sci. 286 (1), 7–13.
Steiger, M., 2005. Crystal growth in porous materials—I: the crystallization pressure of large crystals. J. Cryst. Growth 282 (3–4), 455–469.
Tahmasebi, H.A., Kharrat, R., Soltanieh, M., 2010. Dimensionless correlation for the prediction of permeability reduction rate due to calcium sulphate scale deposition in carbonate grain packed column. Journal of the Taiwan Institute of Chemical Engineers 41 (3), 268–278.
Todd, A., Yuan, M., 1992. Barium and strontium sulfate solid-solution scale formation at elevated temperatures. SPE Prod. Eng. 7 (1), 85–92, 0.
Troup, D., Richardson, J., 1978. Scale nucleation on a heat transfer surface and its prevention. Chem. Eng. Commun. 2 (4–5), 167–180.
Tung, N.P., Phong, N.T.P., Long, B.Q.K., Duy, N.H., 2004. Scale inhibitors for co-deposited calcium sulfate and calcium carbonate in squeeze process in white tiger oilfield. In: Paper Presented at the SPE International Symposium on Oilfield Scale.
Van Domelen, M.S., Jennings Jr., A.R., 1995. Alternate acid blends for HPHT applications. In: Paper Presented at the Offshore Europe.
Verdoes, D., Kashchiev, D., Van Rosmalen, G., 1992. Determination of nucleation and growth rates from induction times in seeded and unseeded precipitation of calcium carbonate. J. Cryst. Growth 118 (3–4), 401–413.
Wang, H., Alfredsson, V., Tropsch, J., Ettl, R., Nylander, T., 2013a. formation of CaCO3 deposits on hard Surfaces effect of bulk solution conditions and surface properties. ACS Appl. Mater. Interfaces 5 (10), 4035–4045.
Wang, Q., Ajwad, H., Shafai, T., Lynn, J.D., 2013b. Iron sulfide scale dissolvers: how effective are they?. In: Paper Presented at the SPE Saudi Arabia Section Technical Symposium and Exhibition.
Wang, Z., Neville, A., Meredith, A., 2005. How and why does scale stick-Can the surface be engineered to decrease scale formation and adhesion?. In: Paper Presented at the SPE International Symposium on Oilfield Scale.
Yan, F., Zhang, F., Bhandari, N., Wang, L., Dai, Z., Zhang, Z., Liu, Y., Ruan, G., Kan, A., Tomson, M., 2015. Adsorption and precipitation of scale inhibitors on shale formations. J. Petrol. Sci. Eng. 136, 32–40.
Zahedzadeh, M., Karambeigi, M., Roayaei, E., Emadi, M., Radmehr, M., Gholamianpour, H., Ashoori, S., Shokrollahzadeh, S., 2014. Comprehensive management of mineral scale deposition in carbonate oil fields–A case study. Chem. Eng. Res. Des. 92 (11), 2264–2272.
Zhang, Y., Farquhar, R., 2001. Laboratory determination of calcium carbonate scaling rates for oilfield wellbore environments. In: Paper Presented at the International Symposium on Oilfield Scale.